

# Advances in Radiance Field for Dynamic Scene: From Neural Field to Gaussian Field

Jinlong Fan, Xuepu Zeng, Jing Zhang, Mingming Gong, Yuxiang Yang, Dacheng Tao

**Abstract**—Dynamic scene representation and reconstruction have undergone transformative advances in recent years, catalyzed by breakthroughs in neural radiance fields and 3D Gaussian splatting techniques. While initially developed for static environments, these methodologies have rapidly evolved to address the complexities inherent in 4D dynamic scenes through an expansive body of research. Coupled with innovations in differentiable volumetric rendering, these approaches have significantly enhanced the quality of motion representation and dynamic scene reconstruction, thereby garnering substantial attention from the computer vision and graphics communities. This survey presents a systematic analysis of over 200 papers focused on dynamic scene representation using radiance field, spanning the spectrum from implicit neural representations to explicit Gaussian primitives. We categorize and evaluate these works through multiple critical lenses: motion representation paradigms, reconstruction techniques for varied scene dynamics, auxiliary information integration strategies, and regularization approaches that ensure temporal consistency and physical plausibility. We organize diverse methodological approaches under a unified representational framework, concluding with a critical examination of persistent challenges and promising research directions. By providing this comprehensive overview, we aim to establish a definitive reference for researchers entering this rapidly evolving field while offering experienced practitioners a systematic understanding of both conceptual principles and practical frontiers in dynamic scene reconstruction. We maintain an active repository of literature and open-source implementations to complement this survey [here](#).

**Index Terms**—Dynamic Scene Representation, Neural Radiance Field, 3D Gaussian Splatting, Motion Representation, 4D Volume.



## 1 INTRODUCTION

SCENE representation constitutes a fundamental cornerstone in computer vision, with robust 3D scene reconstruction remaining an enduring and vibrant research domain for decades. Recent computational paradigms, catalyzed by advances in 3D representation and differentiable rendering, have reinvigorated methodologies that capture and reconstruct the intricate details of real-world environments. Among these developments, radiance fields have emerged as pivotal representations in 3D vision, particularly through milestone approaches proposed in Neural Radiance Fields (NeRF) [1] and 3D Gaussian Splatting (3D GS) [2]. By coupling these fields with differentiable volumetric rendering [3], analysis-by-synthesis methods have achieved unprecedented fidelity in static scene reconstruction.

However, these early successes predominantly addressed static settings [1, 2, 4, 5, 6, 7], overlooking the inherent dynamics of real-world scenes. In practice, virtually every environment exhibits temporal evolution, whether from object movement, changing illumination, or evolving scene geometry. Recognizing this limitation, numerous recent approaches have extended static radiance field frameworks to handle dynamic scenes and accommodate complex temporal variations [8, 9, 10, 11, 12]. This rapidly expanding corpus of techniques underscores the necessity

for a comprehensive survey synthesizing the state-of-the-art in dynamic scene representation.

The principal challenge in dynamic scene reconstruction lies in accurately modeling the temporal dimension—the motion field. Motion representation constitutes the cornerstone of dynamic scene reconstruction, where the precision of point correspondence across frames directly determines the quality of recovered dynamic content. To address this challenge, our survey begins by systematically examining the taxonomy of motion types and comprehensively reviewing strategies to represent these varies motion in 3D space. Recent advances have demonstrated that continuous and flexible formulations prove especially effective in faithfully representing complex motions without relying on oversimplified discretizations, as evidenced by innovations in neural scene flow fields, deformable radiance fields, and 4D neural volumes [9, 11, 12, 13, 14, 15].

Building upon these motion representations, we analyze diverse strategies for reconstructing and rendering dynamic scenes under various motion conditions from multiple input modalities, including monocular video, multi-view video, and casually captured one. We propose examining these methods from a unified perspective, wherein any dynamic scene can be conceptualized as a static reference space coupled with an appropriate motion representation addressing specific motion types. Furthermore, a significant challenge in this domain involves disentangling the inherent ambiguities between motion, geometry, and appearance. To overcome these ambiguities, researchers frequently employ auxiliary information and regularization techniques as additional supervision or constraints, guiding solutions toward physically plausible and realistic dynamic reconstructions [13, 16, 17, 18, 19, 20, 21, 22, 23].

- J. Fan, X. Zeng, and Y. Yang are with the School of Electronics and Information, Hangzhou Dianzi University, Hangzhou, China (e-mail: {jfan, yyx}@hdu.edu.cn, 2307665474zxp@gmail.com). J. Zhang is with Wuhan University, Wuhan, China (e-mail: jingzhang.cv@gmail.com). M. Gong is with Melbourne Centre for Data Science, School of Mathematics and Statistics, University of Melbourne, Parkville, VIC 3010, Australia (e-mail: Mingming.gong@unimelb.edu.au). D. Tao is with the College of Computing & Data Science at Nanyang Technological University, Nanyang Avenue, 639798, Singapore (e-mail: dacheng.tao@gmail.com).

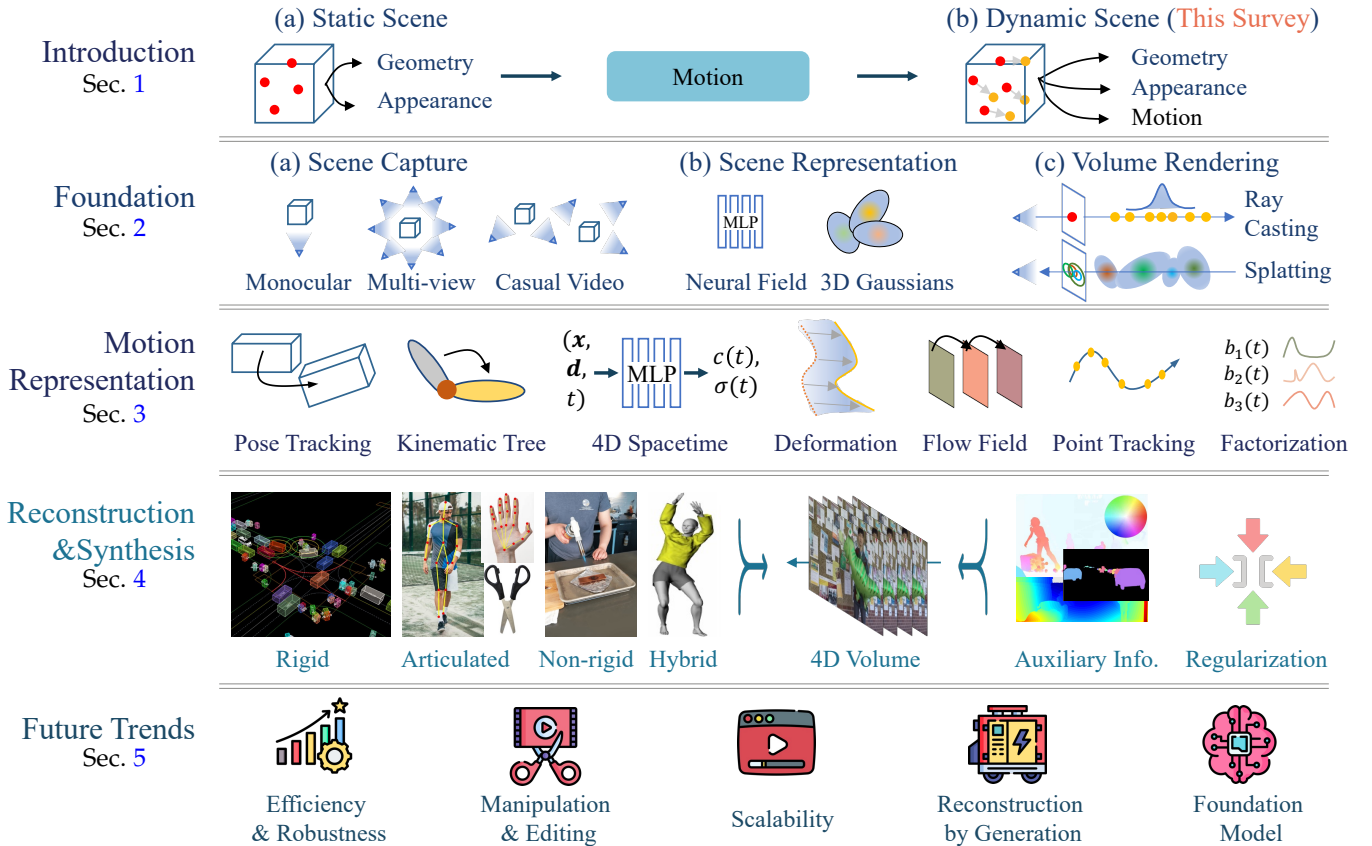


Fig. 1: **Survey at A Glance.** (a) **Introduction and Foundation.** We trace the evolution from static to dynamic scene representation, highlighting the challenges of jointly modeling motion, geometry, and appearance using radiance fields. (b) **Motion Representation.** We categorize motion patterns and their representation paradigms, examining how they enable complex motion modeling while addressing inherent limitations. (c) **Scene Reconstruction.** We analyze how motion representations enable scene reconstruction, discussing these methods within a unified framework while investigating how auxiliary information and regularization strategies constrain the learning of radiance fields. (d) **Future Trends.** We explore promising research directions and how dynamic scene reconstruction could benefit by aid of the rapid development of foundation models, and large language models. Partial photos courtesy of open-source datasets, and online resources.

This survey aims to chart the evolutionary trajectory of dynamic scene representation, highlighting the substantial progress enabled by neural radiance fields and 3D Gaussian splatting while drawing attention to persistent challenges that require further investigation. Figure 1 provides a comprehensive overview of this survey’s structure and scope. By offering a systematically organized examination of recent innovations in motion representation and dynamic scene reconstruction, we seek to provide both newcomers and experienced researchers with valuable insights into emerging directions where dynamic scene modeling can evolve, ultimately facilitating increasingly realistic, interactive, and robust applications across computer vision, graphics, and related fields.

## 1.1 Roadmap

Fig. 2 illustrates the chronological evolution of dynamic scene representation in radiance fields. The journey begins with differentiable volume rendering [24], which enabled gradient-based optimization of 3D-to-2D transformations. A breakthrough came with NeRF [1], which could learn scene representations from only 2D images without 3D

supervision. Early dynamic extensions utilized scene graphs with static and dynamic nodes to handle rigid objects [22, 25, 32], while parametric template-based approaches (using SMPL [33] or MANO [34]) achieved significant success in human avatar reconstruction [30, 35, 36]. For general dynamic scenes, two main paradigms emerged: methods like Nerfies [9] that linked observation space to a canonical space via deformation fields [8, 10], and approaches using frame-to-frame flow fields to establish temporal connections [13, 20, 37, 38]. Subsequently, researchers explored integrated 4D spacetime representations [26, 39, 40, 41], factorization methods for efficient field modeling [14, 15, 42], and techniques like OmniMotion [18] that leveraged long-term dense point tracking.

The field evolved further with the advent of 3DGS [2], which represent 3D scene with Gaussian primitives and rendered through efficient splatting techniques [29]. Replacing implicit neural representations with explicit Gaussian primitives, 3DGS demonstrate great potential for motion modeling. The approaches, that utilizing 3DGS to represent dynamic scenes, fall into several categories: methods that initialize Gaussians at time  $t_0$  as a canonical space and warp

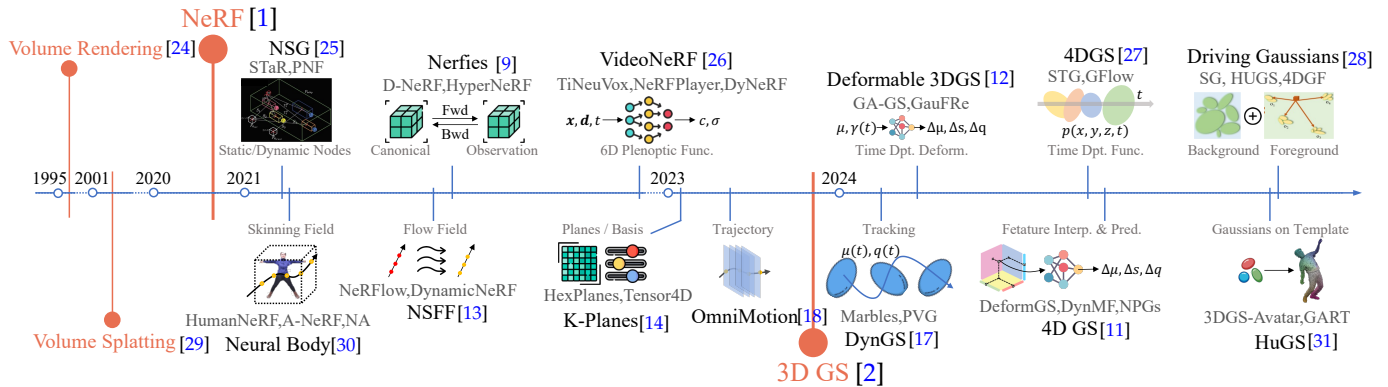


Fig. 2: **Roadmap of Dynamic Scenes in Radiance Fields.** This chronological timeline illustrates the evolution of the field, organizing works into methodological clusters based on their representation paradigms. The representative or first work within each cluster appears in black with accompanying paradigm illustrations, while the dates of remaining works may vary within clusters. Seminal contributions that significantly advanced the field are highlighted with colors.

them using time-dependent deformation fields [12, 43, 44]; techniques that track Gaussian primitive movements to represent dense motion fields [17, 45, 46]; approaches employing time-dependent functions to characterize varying Gaussian properties; and methods utilizing interpolated time-related features on factorized feature planes to predict dynamic Gaussian properties (position, scale, and rotation) [11, 47]. Recent advances have also applied 3D Gaussian fields to represent human avatars [31, 48, 49] and scenes with rigid objects [28, 50, 51, 52], enabling part-level animation or object-level manipulation.

## 1.2 Comparison to Related Surveys

Rapid progress in differentiable rendering and radiance field has led to numerous surveys in this field. The works of [53, 54, 55] provide foundational insight into differentiable rendering, while surveys in [56, 56, 57, 58, 59] document neural radiance field variants. More recently, surveys on 3D Gaussian splatting [60, 61, 62, 63] have emerged to capture developments in explicit representations.

However, a critical gap persists: existing surveys predominantly address static scene representation, with only peripheral coverage of dynamic scenes. Domain-specific surveys [64, 65, 66, 67, 68, 69] incorporate dynamic aspects, but focus on application-specific challenges rather than fundamental problems in dynamic scene representation. Even surveys explicitly addressing non-rigid reconstruction either take a broader view beyond neural fields [70, 71] or focus narrowly on specific scenarios [72, 73, 74]. Our survey distinguishes itself by providing a comprehensive analysis specifically dedicated to dynamic scene reconstruction using radiance fields, including both neural field and 3DGS. We uniquely bridge various representation paradigms within a unified framework, offering a new perspective on this rapidly evolving field.

## 1.3 Contributions

To summarize, this survey has three key contributions: (a) We present a structured roadmap tracing dynamic scene representation from NeRF to 3D Gaussian Splatting, establishing a unified taxonomy of approaches organized

by motion types and representation paradigms. This integrated perspective reveals critical connections between methodological clusters that isolated technical reviews often overlook. (b) We identify fundamental challenges in representing diverse motion patterns based on our survey of over 200 papers. Our analysis examines how different motion representation paradigms address these challenges and how auxiliary information and regularization techniques enhance reconstruction quality and temporal consistency. (c) We analyze how recent breakthroughs in generative and foundation models have transformed the trajectory of dynamic scene reconstruction. To support ongoing research, we maintain an actively updated repository documenting emerging methods, open-source implementations, and benchmark results across the spectrum of dynamic scene representation approaches.

## 2 FOUNDATIONAL CONCEPTS AND KNOWLEDGE

### 2.1 Scene Capture

#### 2.1.1 Sensor Types

Scene capture relies on various sensor types, each with distinct characteristics. **RGB cameras** are the most accessible and widespread sensors, providing dense color information but lacking direct depth measurements, while **RGB-D sensors** enhance this capability by combining RGB data with depth information to simplify 3D reconstruction, though they often suffer from limited range, noise, and sensitivity to environmental conditions. **LiDAR** systems employ laser pulses to generate precise point clouds with accurate geometry, but the resulting data is typically sparse and may require alignment with RGB images before use as auxiliary information in reconstruction pipelines.

#### 2.1.2 Capture Setting

The methodology employed to obtain data substantially influences the quality of dynamic scene reconstruction, affecting both motion fidelity and temporal consistency. Capture settings can be categorized by the number of observation views (single-view, sparse-view, dense-view) or by the capture patterns in the scene (front-view, surrounding-view, or

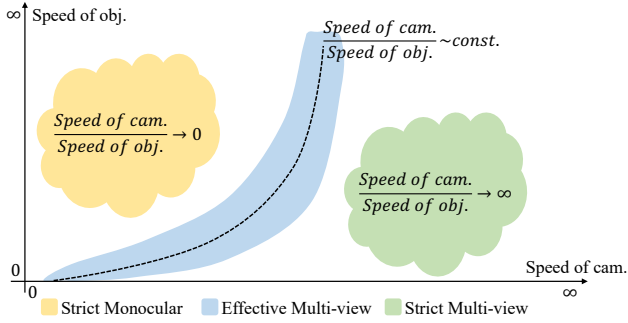


Fig. 3: Relative motion speed between camera and objects determines the critical factor in effective scene capture.

free-view). In this survey, we categorize capture settings into monocular, multi-view, and casual videos.

**Monocular videos** are captured using one camera, which could be stationary (single-view) or moving around (multi-view), but at any given time, only one view is available. As dynamic objects evolve along time, this setting suffers from severe ambiguities in geometry and motion, particularly for occluded regions, making it a challenging scenario for reconstruction.

**Multi-view videos** are captured by synchronized multiple cameras, yielding more comprehensive coverage and fewer occlusions. This configuration provides strong geometric constraints for reconstruction, enabling higher fidelity results but requiring sophisticated hardware setups and careful calibration, which limits its accessibility for everyday applications. Depending on the number of cameras, the system could be sparse or dense, while the position relative to the dynamic object could be front-facing or surrounding, each offering different trade-offs between coverage and complexity.

**Casual videos** are captured using hand-held devices without sophisticated setups, normally in free-view capture patterns and camera poses and parameters are often unavailable. These videos frequently suffer from low quality, motion blur, camera jitter, and complex background distractors that complicate dynamic scene analysis. While this setting offers maximum flexibility and accessibility, it must address not only the challenges of monocular capture (limited views at each timestep) but also the unstable camera setting, more noisy background, requiring robust algorithms for camera tracking, foreground-background separation, and temporal coherence maintenance.

### 2.1.3 Discussion

Dynamic scene reconstruction requires tracking points across video frames, where 2D pixel movement represents a combination of both object and camera motion. The type of sensor setup and capture strategy significantly impacts the system’s ability to accurately estimate true 3D motion, ultimately determining the upper bound of reconstruction outcomes. For static scenes, a single moving camera can provide information equivalent to multiple cameras by capturing different viewpoints over time. However, when objects themselves move, the relationship between camera motion and object motion becomes crucial [75]. This relationship

creates different levels of ambiguity and reconstruction difficulty, categorized as: (1) strict monocular, where the camera moves much slower than objects, creating occlusion challenges, (2) effective multi-view, where camera and object speeds are comparable, allowing the camera to “follow” and maintain visibility of key points, and (3) strict multi-view, where multiple synchronized cameras capture the scene simultaneously from different views. When camera movement closely matches object movement, even single-camera setups can track features effectively enough for reasonable reconstruction, as illustrated in Fig. 3. Importantly, the critical factor is not the absolute motion speed of camera or object, but rather their relative speed ratio.

While strict multi-view camera setups theoretically provide the most complete information for high-quality reconstruction, they introduce practical challenges in synchronization, data management, and deployment complexity. Strict monocular approaches, despite capturing less complete information about the scene, offer significantly simpler solutions for real-world applications. The trade-off between capture complexity and reconstruction quality continues to shift as algorithms improve in handling limited input data, with effective multi-view approaches representing a promising middle ground, making simpler camera setups increasingly viable for many practical uses.

## 2.2 Volumetric Radiance Field

Volumetric radiance fields have emerged as powerful representations for novel view synthesis, offering compelling alternatives to traditional mesh-based or voxel-based scene representations. These approaches encode both geometry and appearance information, enabling photorealistic rendering from arbitrary viewpoints while being directly optimized from multi-view imagery without requiring explicit 3D reconstruction. In this survey, we mainly focus on two prominent implementations: Neural Radiance Fields (NeRF) and 3D Gaussian Splatting.

### 2.2.1 Neural Radiance Field

NeRF [1] represents a scene as a continuous 5D function parameterized by a Multi-Layer Perceptron (MLP) with parameters  $\theta$ , formulated as:

$$\mathcal{F}_\theta(\gamma(\mathbf{x}), \mathbf{d}) \mapsto (\mathbf{c}, \sigma), \quad (1)$$

where  $\mathbf{x} = (x, y, z)$  denotes spatial coordinates,  $\gamma(\cdot)$  is a positional encoding function that maps inputs to higher-dimensional space to capture high-frequency details, and  $\mathbf{d} = (d_x, d_y, d_z)$  represents viewing direction as a normalized unit vector from the camera’s optical center to a pixel position. The network outputs RGB color  $\mathbf{c} = (r, g, b)$  and volume density  $\sigma$ , where density represents view-independent geometry, while color varies with viewing direction to model view-dependent effects such as specular highlights.

**Volume Rendering.** The rendering process in NeRF employs ray tracing principles [24], integrating color and density values along camera rays  $\mathbf{r}(t) = \mathbf{o} + t\mathbf{d}$  to produce the final pixel color. This integration is expressed as:

$$C(\mathbf{r}) = \int_{t_1}^{t_2} T(t) \cdot \sigma(\mathbf{r}(t)) \cdot \mathbf{c}(\mathbf{r}(t), \mathbf{d}) \cdot dt, \quad (2)$$

where transmittance  $T(t) = \exp(-\int_{t_1}^t \sigma(\mathbf{r}(u)) \cdot du)$  represents the probability that light reaches point  $t$  without being occluded by preceding points. In practical implementations, this continuous integral is approximated through stratified sampling, yielding the discrete form:

$$\hat{C}(\mathbf{r}) = \sum_{i=1}^N \alpha_i T_i \mathbf{c}_i, \quad (3)$$

where  $T_i = \exp(-\sum_{j=1}^{i-1} \sigma_j \delta_j)$ ,  $\delta_i$  denotes the distance between adjacent samples, and  $\alpha_i = 1 - \exp(-\sigma_i \delta_i)$  represents the opacity at each sample point.

### 2.2.2 3D Gaussian Splatting

An alternative approach to volumetric scene representation is offered by 3D Gaussian Splatting (3DGS) [2], which employs explicit, learnable primitives rather than implicit neural networks. This method represents scenes as collections of anisotropic 3D Gaussians  $\mathcal{G}$ , each parameterized by its position  $\boldsymbol{\mu} \in \mathbb{R}^3$ , covariance matrix  $\boldsymbol{\Sigma} \in \mathbb{R}^{3 \times 3}$ , opacity  $o \in [0, 1]$ , and color attributes  $\mathbf{c}$ . The covariance matrix, defining the Gaussian’s shape and orientation, is constructed from a scaling factor  $\mathbf{S} \in \mathbb{R}^3$  and rotation matrix  $\mathbf{R} \in \mathbb{R}^{3 \times 3}$  as  $\boldsymbol{\Sigma} = \mathbf{R} \mathbf{S} \mathbf{S}^\top \mathbf{R}^\top$ . The color attributes are typically represented by spherical harmonics (SH) coefficients to model view-dependent appearance effects. All these properties are learnable parameters that are optimized through gradient descent to align with multi-view imagery, allowing the model to accurately represent both geometry and appearance. The explicit nature of this representation offers advantages in terms of interpretability and direct manipulation, though complex scenes may require large numbers of Gaussians, potentially increasing memory requirements.

**Volume Splatting.** Unlike NeRF’s ray marching approach, Gaussian Splatting employs a tile-based rasterization pipeline for efficient rendering [29]. The process involves projecting 3D Gaussian primitives onto the 2D image plane, a technique commonly referred to as "splatting." When projecting each 3D Gaussian, its center is transformed to the 2D image space as  $\boldsymbol{\mu}^{2D} = \mathbf{J} \mathbf{W} \boldsymbol{\mu}$ , and its covariance matrix is similarly transformed to  $\boldsymbol{\Sigma}^{2D} = \mathbf{J} \mathbf{W} \boldsymbol{\Sigma} \mathbf{W}^\top \mathbf{J}^\top$ , where  $\mathbf{W}$  represents the viewing transformation matrix that maps from world to camera coordinates, and  $\mathbf{J}$  is the Jacobian of the affine approximation of the projective transformation.

The final color of each pixel is computed by blending all Gaussian splats that overlap at that pixel location. These Gaussians are first sorted by depth to ensure proper occlusion handling, then composited in front-to-back order according to the equation:

$$\mathbf{c} = \sum_{i \in \mathcal{N}} \mathbf{c}_i \alpha_i^{2D} \prod_{j=1}^{i-1} (1 - \alpha_j^{2D}), \quad (4)$$

where  $\mathcal{N}$  represents the set of Gaussians contributing to the pixel,  $\mathbf{c}_i$  is the color of the  $i$ -th Gaussian, and  $\alpha_i^{2D}$  is the alpha value derived from the Gaussian’s learned opacity  $o_i$  and its 2D projection. This alpha value is calculated as:

$$\alpha_i^{2D} = o_i \exp\left(-\frac{1}{2}(\mathbf{x}^{2D} - \boldsymbol{\mu}_i^{2D})^\top (\boldsymbol{\Sigma}_i^{2D})^{-1} (\mathbf{x}^{2D} - \boldsymbol{\mu}_i^{2D})\right), \quad (5)$$

where  $\mathbf{x}^{2D}$  represents the 2D coordinates of the pixel being rendered.

This splatting-based approach offers significant computational advantages over ray marching, enabling real-time rendering while maintaining high visual fidelity. The explicit nature of the Gaussian primitives also facilitates adaptive density control during optimization, allowing the model to concentrate more Gaussians in complex regions of the scene while using fewer in simpler areas. Moreover, the differentiable nature of the entire pipeline enables end-to-end optimization using only multi-view images as supervision, without requiring explicit 3D ground truth.

### 2.2.3 Discussion

Neural Radiance Fields and 3D Gaussian Splatting represent complementary approaches to volumetric scene representation, each with distinct tradeoffs. NeRF’s implicit continuous representation excels at capturing fine details and complex view-dependent effects through compact network parameters, but requires computationally expensive ray marching that precludes real-time applications. In contrast, 3D Gaussian Splatting’s explicit primitive-based representation enables real-time rendering through efficient rasterization, though complex scenes may demand large numbers of Gaussians that increase memory requirements. The choice between these approaches thus depends on specific application priorities—whether visual fidelity, computational efficiency, or memory constraints takes precedence.

These methods fundamentally differ in their rendering techniques: ray tracing in NeRF provides continuous sampling that accurately captures complex optical phenomena, while splatting in Gaussian representations serves as an approximation of physically-based rendering, sacrificing some fidelity in representing sophisticated light transport effects such as reflections and shadows. This complementarity has motivated recent exploration of hybrid techniques that introduce ray tracing capabilities into Gaussian-based representations to better capture secondary lighting effects while maintaining computational efficiency [76, 77]. As the field advances, developing representations that simultaneously achieve efficiency, fidelity, and real-time performance remains an active frontier in neural rendering, with each approach continuing to inform and enhance the other.

## 3 DYNAMIC MOTION REPRESENTATION

Accurately modeling dynamic motion forms a critical foundation for scene reconstruction, understanding, and analysis. Real-world environments exhibit diverse motion patterns that can be categorized hierarchically from specific to general types. We classify these patterns into rigid motion, articulated motion, general non-rigid motion, and hybrid motion (which combines multiple patterns). Although articulated motion represents a specific type of non-rigid movement, we address it separately due to its distinct representation approaches [78]. Throughout this survey, we use the term "non-rigid" to describe more general deformation patterns beyond articulated movement.

The primary objective in motion representation is to establish accurate correspondences of 3D points across successive temporal frames. Formally, given a point  $\mathbf{x}_{t-1} \in \mathbb{R}^3$  at time  $t-1$ , its position  $\mathbf{x}_t$  at time  $t$  can be described by:

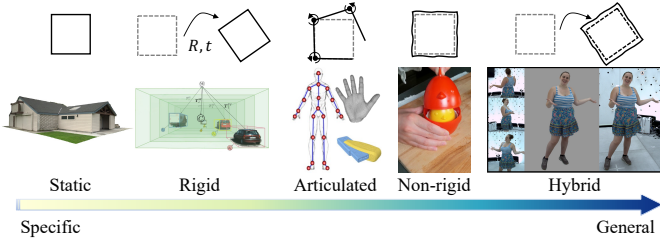


Fig. 4: A 2D illustration of various motion types with representative examples.

$$\mathbf{x}_t = \mathcal{T}_\theta(\mathbf{x}_{t-1} \mid \pi), \quad (6)$$

where  $\mathcal{T}_\theta(\cdot)$  is a transformation function parameterized by  $\theta$  and conditioned on temporal context  $\pi$  (e.g., time  $t$ , frame index  $i$ , embeddings  $\ell_t$ , or motion-specific parameters). The precise form of  $\mathcal{T}_\theta(\cdot)$  depends on the underlying motion pattern and representation method, typically involving different assumptions and formulations.

### 3.1 Motion Types

#### 3.1.1 Rigid Motion

Rigid motion encompasses transformations in which an object preserves its shape and size while undergoing rotation and translation. Internally, distances and angles remain unchanged, and thus no deformation occurs. This can be mathematically expressed via a rotation matrix  $\mathbf{R} \in SO(3)$  (or quaternion  $\mathbf{q} \in \mathbb{R}^4$ ) and a translation vector  $\mathbf{t} \in \mathbb{R}^3$ , such that:

$$\mathbf{x}_t = \mathcal{T}_\theta(\mathbf{x}_{t-1}) = \mathbf{R}\mathbf{x}_{t-1} + \mathbf{t}. \quad (7)$$

Rigid objects are ubiquitous in daily life, including furniture like boxes and chairs, kitchenware, and other manufactured items. Additionally, certain objects such as vehicles, though not strictly rigid, can be effectively approximated as rigid bodies for many applications, as they maintain a relatively fixed internal structure while translating or rotating [64]. In dynamic view synthesis, accurately tracking and updating an object’s rigid 6DoF pose across frames ensures correct rendering from novel viewpoints [51, 79, 80].

#### 3.1.2 Articulated Motion

Articulated motion, also known as piecewise rigid motion, describes a class of transformations where individual segments (e.g., limbs in a skeletal model) undergo rigid transformations while the object’s overall motion appears non-rigid due to the relative movement between segments. This type of motion is ubiquitous in both natural organisms (human and animal skeletons) and manufactured systems (robotic arms, mechanical assemblies, and hinged objects).

An articulated object is typically represented by a kinematic tree—a hierarchical structure of rigid segments connected by joints that provide specific degrees of freedom (e.g., rotation or translation). This hierarchical organization captures how local transformations at each joint propagate through the kinematic chain. The human body represents a quintessential example of such articulated structures, and

various parameterization strategies, such as SCAPE [81], SMPL [33], SMPL-X [82], and MANO [34], have produced influential frameworks for modeling its complex motion. Among these, the Skinned Multi-Person Linear Model (SMPL) has gained particular prominence due to its balance of expressiveness and computational efficiency.

SMPL conceptualizes the human body as a kinematic tree with 24 joints, each undergoing a rigid transformation relative to its parent, with the root joint defining the transformation from the body’s local space to world space. The model employs linear blend skinning (LBS) to deform a canonical rest pose according to a target pose configuration. By assigning blend weights to each vertex on a canonical mesh, SMPL effectively encodes how much each joint’s transformation influences that point. Formally, for a point  $\mathbf{x}_i^c$  in the canonical space, its deformed position  $\mathbf{x}_i^p$  in the posed space is computed by:

$$\mathbf{x}_i^p = \mathcal{T}_\theta(\mathbf{x}_i^c; (\mathbf{x}_i^c), \pi(J)) = \sum_{j=1}^J (w_j(\mathbf{x}_i^c) T_j) \mathbf{x}_i^c, \quad (8)$$

where  $\pi(J)$  represents the joint pose parameters,  $w_j(\mathbf{x}_i^c)$  are blend weights determining joint  $j$ ’s influence on point  $\mathbf{x}_i^c$ , and  $T_j \in \mathbb{R}^{4 \times 4}$  is the rigid transformation matrix of the  $j$ -th joint. SMPL predefines these blend weights on a canonical mesh parametrized by a shape code  $\beta$ , allowing for personalized body proportions.

While LBS accurately describes transformations for points on the template surface, handling points in free space (e.g., for volumetric rendering) requires additional techniques. Traditional approaches use barycentric interpolation or nearest-neighbor methods to extend blend weights to off-surface points [30, 36, 83]. However, these approaches may struggle with complex deformations, especially for loose clothing or accessories. To address these limitations, recent approaches employ neural skinning fields that replace or augment traditional pre-defined blend weights. A learnable skinning function maps a point  $\mathbf{x}$  to its joint-influence weights:

$$\mathcal{W}(\mathbf{x}) = \mathcal{S}_\theta(\mathbf{x}, \pi(t)), \quad (9)$$

where  $\pi(t)$  encodes time-dependent variations. Learning such fields from scratch presents challenges; therefore, many methods incorporate the pre-defined SMPL blend weights as a strong prior, allowing the learned skinning weights to deviate moderately from the canonical configuration when necessary [35, 84].

#### 3.1.3 Non-Rigid Motion

Non-rigid motion permits objects to deform by locally changing the relative positions of points and is therefore indispensable for describing cloth folding, facial expression, fluid flow, and other complex dynamics. Unlike rigid or articulated motion, which can exploit kinematic templates or low-dimensional parametric models, general non-rigid deformation typically lacks structured representations due to potential topology changes and the infinite degrees of freedom involved. Classical tracking pipelines rely on sparse feature matching, yielding motion fields that are far too coarse to capture fine-scale deformation. Physically

based methods may provide accurate solutions, yet their computational cost becomes prohibitive for large scenes or real-time use.

Recent advances have reformulated non-rigid motion as an implicit, learnable neural field. These approaches employ compact neural networks  $\Delta_\theta$  to predict dense, continuous displacement fields of the form:

$$\mathbf{x}_t = \mathbf{x}_{t-1} + \Delta_\theta(\mathbf{x}_{t-1}; \pi(t)). \quad (10)$$

where  $\Delta_\theta$  maps any 3D point at time  $t-1$  to its offset at time  $t$ , conditioned on a temporal code  $\pi(t)$ . Such neural fields can be trained directly from 2D images through differentiable rendering, dispensing with explicit 3D supervision and delivering per-point motion estimates. The learning problem, however, is ill-posed—especially under monocular observations—because many distinct deformations can explain the same pixel sequence. Contemporary systems therefore narrow the solution space with a hierarchy of priors. Geometric regularizers promote smooth, continuous flows and discourage fold-overs or self-intersections [13]; isotropy or near-rigidity assumptions penalize changes in pairwise distances [49, 85]; additional 2D cues such as dense optical flow or sparse feature correspondences supply direct motion evidence [19, 86]; and, when multi-view images are available, cross-view consistency enforced via neural rendering further suppresses spurious solutions [87]. A detailed discussion of these auxiliary cues and their implementation appears in Sec. 4.5.

### 3.1.4 Hybrid Motion

Most real-world scenes exhibit a mixture of motion types—rigid, articulated, and general non-rigid—whose simultaneous presence gives rise to hybrid motion. A prime example is the human body: a primarily articulated skeleton undergoes a global rigid transformation, while soft tissue, loose clothing, and hair introduce finer, highly deformable dynamics [88, 89]. Capturing this interplay demands a representation that is both structured enough to model global motion and flexible enough to accommodate local deviations.

Contemporary approaches typically factorize the total motion into complementary components:

$$\mathbf{x}_t = \underbrace{\mathcal{T}_{\theta_1}(\mathbf{x}_{t-1}; \pi(t))}_{\text{coarse, e.g. rigid/articulated}} + \underbrace{\Delta_{\theta_2}(\mathbf{x}_{t-1}; \pi(t))}_{\text{fine, e.g. non-rigid residual}}. \quad (11)$$

In this formulation,  $\mathcal{T}_{\theta_1}$  represents a relatively constrained, interpretable global motion model (e.g., rigid transformation or articulated skeleton deformation), while  $\Delta_{\theta_2}$  is typically implemented as a neural field that predicts residual displacements to capture complex, local deformations. Besides effective human and animal modeling, similar approaches have been applied to other domains with composite motion, including deformable objects with near-rigid parts and multi-object scenes with varying motion characteristics [51, 80]. This hierarchical decomposition offers several advantages: it maintains physical interpretability by isolating well-defined transformations; it reduces the complexity of the learning problem by having the neural component focus on residual details rather than the entire

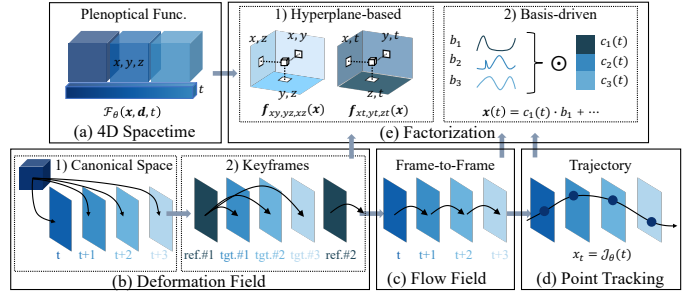


Fig. 5: Illustration of typical motion representation methods. An intuitive approach extends the 5D plenoptic function to 6D by incorporating time  $t$  as an additional dimension, creating a **4D Spacetime** (a) representation. Alternative methods represent the scene as a shared reference space and time-dependent **Deformation Fields** (b). This reference can be a globally shared **Canonical Space** (b-1) consistent across the entire video, or **Keyframes** (b-2) shared locally among neighboring frames. When each frame serves as the keyframe for its successive frame, the representation becomes a frame-to-frame **Flow Field** (c). **Point Tracking** (d) continuously integrates point trajectories across frames, rather than using discrete frame-to-frame correspondences. **Factorization** (e) approaches decompose 4D spacetime into **Hyperplanes** (e-1) or represent complex motion using low-rank **Basis** (e-2) functions, effectively reducing dimensionality while preserving motion characteristics.

motion; and it provides explicit control over coarse motion while allowing data-driven capture of fine details such as clothing wrinkles, or facial expressions. Despite implementation challenges in properly balancing and integrating different motion representations, hybrid approaches remain essential for high-fidelity dynamic scene reconstruction, realistic animation, and applications requiring both structural accuracy and fine detail preservation.

## 3.2 Motion Representation

### 3.2.1 Representing via 4D Spacetime

Starting from coordinate-based representations for static scenes [1], which utilize the 5D plenoptic function to represent light fields as  $\mathcal{F}_\theta: (\mathbf{x}, \mathbf{d}) \mapsto (\mathbf{c}, \sigma)$ , approaches for dynamic scenes naturally extend the input domain to 6D by incorporating temporal information  $t$  [16, 26, 40, 90], resulting in  $\mathcal{F}_\theta: (\mathbf{x}, \mathbf{d}, t) \mapsto (\mathbf{c}, \sigma)$ . More generally, methods may condition on alternative temporal encodings beyond direct time input, such as frame indices  $i$  or learned per-frame latent codes  $\ell_i$  [41, 91, 92].

With this formulation, each frame of the dynamic scene is optimized independently through frame-by-frame optimization, leveraging multi-view observations to minimize a rendering loss between the synthesized output  $I_r$  and the ground-truth image  $I_{gt}$ :

$$\arg \min_{\theta} \sum \|I_r - I_{gt}\|_2^2, \text{ where } I_r = \mathcal{R}(\mathcal{F}_\theta(\mathbf{x}, \mathbf{d}, \pi(t))), \quad (12)$$

where  $\mathcal{R}$  represents a differentiable volume rendering function (e.g., ray tracing),  $\mathcal{F}_\theta$  denotes the radiance field with learnable parameters  $\theta$ , and  $\pi(t)$  encodes temporal

information. Motion is thus implicitly encoded within the same radiance field that represents the scene—rather than being handled by a dedicated motion module—and is supervised solely through available 2D image observations.

While this 4D spacetime representation with frame-by-frame optimization can produce high-fidelity reconstructions at individual time steps, it suffers from notable limitations. Using a single time-related variable to represent frame-level motion makes these models can not provides explicit point-level motion information. Furthermore, without an explicit 3D scene model, maintaining cross-view consistency between novel viewpoints becomes challenging. Despite these limitations, 4D spacetime representations remain central in many dynamic scene reconstruction pipelines, particularly when memory efficiency and 4D video compression are priorities.

### 3.2.2 Representing via Canonical Space with Deformation Field

A prevalent approach for modeling dynamic scenes decomposes the representation into a static canonical space and time-varying deformation fields. This canonical space—often designated as a "reference frame"—serves as a common coordinate system from which all observed frames are derived through learned deformations. For rigid or articulated objects, this canonical space typically corresponds to a rest pose (e.g., initial frame or neutral skeletal configuration). For non-rigid scenes, it should capture sufficient geometric detail to facilitate robust correspondence estimation across the sequence.

The relationship between the canonical space and each observation frame is formalized through deformation fields implemented as neural networks. A forward deformation field  $\Phi_\theta$  maps points from canonical space to the observation space at time  $t$ :

$$\Delta_{c \rightarrow i}(\mathbf{x}_c) = \Phi_\theta(\mathbf{x}_c; \pi(t)), \quad (13)$$

Conversely, a backward deformation field  $\Psi_\theta$  maps observation space points back to canonical space:

$$\Delta_{i \rightarrow c}(\mathbf{x}_i) = \Psi_\theta(\mathbf{x}_i, \pi(t)). \quad (14)$$

These fields should ideally satisfy invertibility, where  $\Phi_\theta \equiv \Psi_\theta^{-1}$ , ensuring consistent bidirectional mappings between spaces. This constraint is typically enforced through inverse-consistency regularization or explicitly using invertible neural architectures [18, 93, 94].

Within this framework, motion between any two observation frames  $i$  and  $j$  can be computed via the canonical space:

$$\Delta_{i \rightarrow j} = \Delta_{i \rightarrow c} + \Delta_{c \rightarrow j}, \quad (15)$$

For scenes with complex motions or topology changes where a single global canonical space becomes impractical, other approaches employ multiple local canonical spaces or keyframes that serve as reference frames for temporal sub-windows [41, 95]. This extension enables the representation of longer sequences with more complex dynamics.

By decoupling the scene into a static reference space and time-dependent deformations, this framework accommodates diverse motion types ranging from rigid transformations to fully non-rigid deformations. It also facilitates transparent analysis and manipulation of motion—valuable in medical applications tracking tissue deformation and entertainment contexts requiring precise animation control. The explicit modeling of deformations further enables motion transfer, pose editing, and novel pose synthesis applications that are challenging with implicit spacetime representations.

### 3.2.3 Representing via Flow Field

A more direct strategy for modeling dynamic scenes involves capturing motion between consecutive frames rather than relating observations to a canonical space. This frame-to-frame approach leverages incremental deformations to represent complex motions, decomposing significant transformations into smaller, more tractable steps. Such representations naturally accommodate topology changes and extreme deformations that challenge canonical space methods.

Flow fields provide a principled framework for modeling these consecutive-frame dynamics. In their continuous form, velocity fields [19, 50, 96] specify instantaneous motion by assigning a velocity vector  $\mathbf{v}(\mathbf{x}, t)$  to each point  $\mathbf{x}$  in space at time  $t$ . The trajectory of a point initially at position  $\mathbf{x}_{t-1}$  can be computed by integrating this velocity field:

$$\mathbf{x}_t = \mathbf{x}_{t-1} + \int_{t-1}^t \mathbf{v}(\mathbf{x}(\tau), \tau) d\tau, \quad (16)$$

where  $\mathbf{v}(\mathbf{x}(\tau), \tau)$  represents the velocity at intermediate time  $\tau$ . While theoretically elegant, obtaining dense ground-truth velocities in practical settings is often infeasible.

For discrete time steps, scene flow fields  $\Phi(\mathbf{x}, t)$  directly model displacement vectors between consecutive frames:

$$\Phi(\mathbf{x}, t) = \mathbf{x}_t - \mathbf{x}_{t-1}. \quad (17)$$

Scene flow and velocity fields are mathematically related—velocity represents the time derivative of scene flow—expressed differentially as:

$$\frac{\partial \Phi}{\partial t}(\mathbf{x}, t) = \mathbf{v}(\Phi(\mathbf{x}, t), t), \quad \text{s.t.} \quad \Phi(\mathbf{x}, t-1) = \mathbf{x}_{t-1}, \quad (18)$$

In practical implementations, both fields are typically parameterized by neural networks and optimized through differentiable rendering pipelines.

The frame-to-frame motion between frames  $i$  and  $j$  is expressed as:

$$\Delta_{i \rightarrow j} = \Phi_\theta(\mathbf{x}, \pi(t_i)). \quad (19)$$

These local flow fields can be composed to represent extended trajectories through:

$$\Delta_{i \rightarrow k} = \Delta_{i \rightarrow j} + \Delta_{j \rightarrow k}, \quad (20)$$

with inverse mappings defined as  $\Delta_{j \rightarrow i} \equiv \Delta_{i \rightarrow j}^{-1}$ .

This frame-to-frame paradigm offers two significant advantages. First, it operates on incrementally small displacements that neural networks can more effectively learn and generalize across diverse scenarios. Second, it eliminates the need for a global canonical space—often problematic under

significant deformations or topology changes. These properties make flow-based representations particularly suitable for complex non-rigid dynamics where corresponding points may appear, disappear, or undergo substantial deformation throughout a sequence.

### 3.2.4 Representing via Point Tracking

Recovering motion ultimately reduces to establishing reliable point correspondences across time. Early solutions include sparse feature matching and optical flow. Sparse feature matching identifies distinctive keypoints that can be matched across views and has fueled SfM and SLAM pipelines [97]. While effective for camera pose estimation and rigid-scene reconstruction, these sparse correspondences reveal little about dense, non-rigid dynamics. Optical flow extends this by estimating dense 2D correspondences between successive frames [98, 99, 100], but long-range tracking quickly deteriorates under appearance changes, occlusions, or large viewpoint shifts.

To extend temporal support, several works chain short-term matches into longer 2D point trajectories [101, 102, 103]. However, purely image-plane tracking struggles with out-of-plane motions that are more naturally handled in 3D. Scene-flow methods (Sec. 3.2.3) lift correspondences to 3D but restricts motion to adjacent frames.

Recent progress in differentiable volume rendering has enabled dense, long-term 3D tracking driven only by 2D supervision [17, 18, 23]. These approaches jointly optimize a volumetric scene representation and a continuous trajectory field:

$$\mathbf{x}_t = \mathcal{J}_\theta(t), \quad (21)$$

where  $\mathcal{J}_\theta$  returns the 3D position of a point at any time  $t$ . Trajectories can be realized by composing deformation fields through a canonical space (Eq. 15) or by integrating consecutive flow fields (Eq. 20). Rather than stitching these local matches, several methods fit  $\mathcal{J}_\theta$  directly over the full sequence, enforcing temporal smoothness and consistency [45, 46]. At the meantime, foundation models such as DINO [104] can also supply robust, semantically rich features that could further stabilize long-range correspondence under severe appearance change. Trajectory-based tracking thus provides a unified motion description in which every scene point follows a continuous 3D path.

### 3.2.5 Representing via Factorization

Decomposing high-dimensional, complex signals into lower-dimensional, simpler components represents a fundamental strategy for efficient scene representation. This approach significantly reduces computational complexity while preserving essential scene characteristics. For static neural radiance fields, methods such as TensorRF [5] and EG3D [105] have demonstrated the effectiveness of this principle by representing 3D space using 2D tensors and triplanes, achieving both efficient training and rendering.

When extending to dynamic scenes, the 4D spacetime domain introduces additional complexity that can be effectively managed through factorization techniques. Methods like Hexplane [15] and K-planes [14] decompose this 4D domain into separable components: static spatial features

captured in planes  $(\mathbf{f}_{xy}, \mathbf{f}_{yz}, \mathbf{f}_{xz})$ , and motion-related temporal components represented in planes  $(\mathbf{f}_{xt}, \mathbf{f}_{yt}, \mathbf{f}_{zt})$ . For any 3D point  $\mathbf{x}$  at a specific time  $t$ , its features are interpolated from these orthogonal planes and processed by a neural network to predict the radiance field properties:

$$\mathcal{F}_\theta(\mathbf{f}_{xy,yz,zx}(\mathbf{x}), \mathbf{f}_{xt,yt,zt}(\mathbf{x})) \mapsto (\mathbf{c}, \sigma). \quad (22)$$

This hyperplane-based factorization effectively disentangles spatial and temporal components, enabling more efficient optimization and better generalization across the temporal domain.

For scenarios where motion is modeled separately—such as in deformation fields or flow fields—a basis-driven decomposition provides an elegant solution. This approach leverages a limited set of shared motion bases  $\{\mathbf{b}_i\}_{i=1}^B$  and time-dependent coefficients  $c_i(t)$  to represent each point’s motion trajectory:

$$\mathbf{x}(t) = \sum_{i=1}^B c_i(t) \mathbf{b}_i, \quad \text{with } \mathbf{b}_i \in \mathbb{R}^3, \quad c_i(t) \in \mathbb{R} \quad (23)$$

This formulation is particularly powerful because in real-world scenes, nearby points often share similar motion patterns. Since the number of basis functions  $B$  is typically much smaller than the number of points in the scene, this creates a well-constrained factorization problem that enhances regularization and temporal consistency.

The shared basis vectors  $\mathbf{b}_i$  can be implemented as learnable parameters or derived from orthogonal function families such as Fourier or sinusoidal expansions. The coefficients  $c_i(t)$  dynamically weight each basis vector’s contribution to a point’s overall displacement. Both the basis vectors and coefficients can be jointly optimized with scene geometry and appearance, creating a unified representation that maintains global consistency over time.

This basis-driven approach offers several advantages: it significantly reduces the parameter space required to represent complex dynamic scenes, enforces motion coherence between spatially proximate points, and enables smoother interpolation for novel time steps. By leveraging the underlying structure in real-world motion, these factorization techniques provide a scalable and efficient framework for modeling complex 4D dynamics.

## 3.3 Discussion

Dynamic scene representation presents fundamental challenges, particularly when reconstructing complex motions from limited observations in monocular or sparse view settings. The efficacy of different representation paradigms varies significantly across motion types, with no single approach universally excelling across all scenarios. Rigid motion, efficiently modeled through pose tracking, represents objects using low-dimensional transformations (rotation and translation), making it computationally efficient and interpretable. The key challenge lies in accurately aligning tracking results at different timestamps within a common coordinate system to aggregate temporal information effectively. Articulated motion extends this concept by representing hierarchical relationships between connected rigid parts through kinematic tree structures, balancing

Method	Venue	Input	Auxiliary				Motion rep.	Scene rep.
			Lidar	Depth	Seg.	O.F.		
NSG [25]	CVPR'21	stereo					scene graph	MLP
STaR [32]	CVPR'21	multi-view					learnable pose	MLP
PNF [22]	CVPR'22	monocular			✓		pose tracking	MLP
Mars [106]	CICIA'23	monocular		✓	✓		pose tracking	MLP/voxel
UniSim [107]	CVPR'23	monocular	✓				scene graph	feature grids
S-NeRF [108]	ICLR'23	multi-view	✓		✓	✓	learnable pose	MLP
ProSGNeRF [109]	Arxiv'23	monocular			✓		pose tracking	MLP
ML NSG [110]	CVPR'24	monocular	✓				scene graph	MLP
HUGS [50]	CVPR'24	monocular			✓	✓	unicycle model	3DGS
SG [52]	ECCV'24	monocular	✓				learnable pose	3DGS
NeuRAD [111]	CVPR'24	monocular	✓				pose tracking	MLP
DrivingGaussian [28]	CVPR'24	multi-view	✓		✓		scene graph	3DGS
AutoSplat [112]	ICRA'25	monocular	✓		✓		pose tracking	3DGS

TABLE 1: Selected papers for dynamic scene reconstruction with rigid motion.

strong priors with sufficient flexibility to model entities like humans and animals, though typically requiring category-specific templates that limit broader application.

Non-rigid motion encompasses more general deformations without the structural constraints of rigid or articulated motion, leading to diverse representation strategies with varying strengths. Fig. 5 illustrates the typical representation methods. The 4D spacetime representation directly extends static radiance fields to temporal domain for frame-by-frame optimization, offering conceptual simplicity but lacking explicit point-level motion information and struggling with temporal consistency. Canonical space with deformation fields elegantly disentangles structure from motion by decomposing dynamic scenes into a static canonical space and time-varying deformation fields, though defining appropriate canonical spaces becomes challenging for sequences with large deformations. For longer sequences with significant changes, keyframe-based approaches replace a single canonical space with multiple reference frames, better accommodating topology changes at the cost of increased memory requirements.

Frame-to-frame flow fields model incremental deformations between consecutive frames, naturally accommodating topology changes without requiring global canonical spaces, though they struggle with establishing long-range correspondences and may accumulate errors over time. Point tracking approaches represent each point’s motion as a continuous function across time, establishing dense 3D correspondences but remaining vulnerable to occlusions. Factorization-based representations decompose motion into a limited set of shared basis and time-dependent coefficients, effectively capturing common motion patterns while reducing dimensionality and computational complexity, making complex motion field regularization more intuitive through coefficient regularization.

These representations exist on a spectrum balancing structure and flexibility, with rigid and articulated representations imposing strong priors but sacrificing adaptability, while frame-by-frame approaches maximize flexibility at the cost of temporal consistency. For real-world applications, hybrid approaches combining multiple representation paradigms often yield superior results.

## 4 DYNAMIC SCENE RECONSTRUCTION

### 4.1 Reconstructing with Rigid Motion

Rigid motion reconstruction fundamentally revolves around pose tracking—estimating the 6DoF transformation of each object over time. By tracking the 3D bounding boxes of moving objects, these methods spatially decomposes dynamic scenes into foreground objects and static backgrounds [52], with some methods incorporating dedicated sky modules to handle distant, uncertain regions [106]. Early works such as NSG [25] introduced scene graphs—hierarchical structures where nodes represent individual scene elements (objects or background) and edges encode their spatial relationships as rigid transformation, enabling efficient novel view synthesis of complex dynamic scenes. This concept evolved into multi-level scene graph in ML NSG [110] and dynamic scene graph in ProSGNeRF [109]. Multi-view systems like STaR [32] employ self-supervised tracking alongside scene graphs to jointly optimize object poses and appearances without manual annotations.

Temporal coherence is achieved by linking object instances across frames through consistent pose tracking. Methods like PNF [22] additionally employ meta-learning techniques to initialize category-specific object fields, while HUGS [50] constrains vehicles to ground-plane motion using a unicycle model for improved stability. More recent approaches such as S-NeRF [108] and SG [52] optimize tracked poses jointly with scene parameters, yielding more accurate reconstruction and alignment across frames.

A recent trend is the transition from implicit neural radiance fields (parameterized by MLPs) to explicit 3DGS representations for faster convergence and real-time rendering capabilities. To constrain the ill-posed nature of dynamic scene reconstruction (especially from monocular inputs), methods often leverage auxiliary information such as semantic segmentation [22, 28, 50, 106, 112], optical flow [50, 108], or Lidar [111, 112] and depth data [106] to offer precise boundary, constrain motion space, and resolve scale ambiguity or employ meta-learning techniques to initialize category-specific object fields [22]. UniSim [107] further incorporate feature grids to model finer environmental details while maintaining efficient object-level motion representation.

The practical applications of these approaches span autonomous driving, augmented reality, and robotics. Explicit scene decomposition through rigid motion tracking enables

capabilities like object removal [25], trajectory modification [111], and viewpoint manipulation [107]—all crucial for simulation environments and digital twins.

## 4.2 Reconstructing with Articulated Motion

**Human body:** Articulated human body reconstruction has evolved through distinct developmental stages, progressing from simple 2D/3D pose estimation and basic mesh recovery [138] toward photorealistic appearance and fine geometric detail reconstruction. This advancement has been particularly accelerated by the introduction of implicit neural fields [139, 140], especially neural radiance fields [1, 2], which enable high-fidelity modeling of complex human bodies. Early reconstruction approaches strategically integrated parametric human models such as SMPL or SMPL-X as structural priors with neural radiance fields to represent time-varying surface details. These methods established the canonical space paradigm—where the human body is represented in a standardized rest pose while points from the observation space (posed body) are transformed to this canonical reference frame via inverse skinning to query appearance properties like color and density values [35, 115, 116, 117, 141].

The radiance field is supervised using multi-view or monocular images, with the optimization accounting for both appearance and geometry. A fundamental challenge is diffusing skinning weights—originally defined only on the parametric mesh surface—to arbitrary points in 3D space. Solutions range from nearest-neighbor interpolation [83, 114, 142] and barycentric mapping [36] to more sophisticated approaches like Neural Body’s 3D convolutional networks and learnable continuous skinning fields [84, 143, 144]. While early methods defined skinning fields in observation space, these approaches frequently struggle with generalization to novel poses [145, 146]. Recent advances define skinning in canonical space and employ root-finding algorithms to establish bidirectional point correspondences [84, 95, 144, 147, 148], enabling forward skinning transformations that generalize significantly better to out-of-distribution poses and providing more robust reconstruction across complex articulations. Complementary techniques include pixel-aligned features for cross-identity generalization [116, 149, 150, 151], part-wise representations for enhanced detail [148], and hybrid representation for more efficient training and rendering [144, 152, 153].

3D Gaussian Splatting (3DGS) has emerged as a transformative explicit representation for articulated human bodies, offering both quality improvements and dramatic efficiency gains over implicit neural fields [31, 48, 118, 119, 120, 122, 154, 155]. In a typical 3DGS pipeline, Gaussians are initialized based on a parametric template in rest pose and then transformed into observation space via forward skinning, which naturally drives both position and orientation parameters. During this skinning process, the color and density of the Gaussians are typically fixed as initialized to ensure better convergence [49]. This approach fundamentally resolves the correspondence ambiguities present in inverse skinning used by neural implicit representations. Instead of directly optimizing Gaussian parameters, some methods represent Gaussians with learned embeddings,

predicting parameters using embeddings sampled via UV mapping [120, 121, 122]. As 3D Gaussian fields lack inherent structure, advanced methods bind Gaussians to structured meshes or tetrahedral cages to enhance animation control and spatial coherence [156, 157]. Several approaches also jointly optimize pose, skinning weights, and skeletal structures alongside Gaussian parameters [158].

Beyond canonical space methods, alternative approaches represent articulated bodies directly in observation space or pursue template-free reconstruction. Direct observation space techniques leverage specialized parameterizations such as UV-based coordinates [36, 159] or skeleton-based local coordinates [113, 114, 160], circumventing the need for explicit canonicalization. Meanwhile, template-free approaches learn articulation parameters—including skeleton structures and skinning weights—entirely from scratch, demonstrating remarkable generalizability across different body types and motion patterns [123, 161, 162]. These methods typically incorporate auxiliary supervision from silhouettes, semantic segmentation, optical flow, or leverage data-driven priors from foundation models like DINO features [104] or CSE embeddings [163] to establish robust correspondences across frames. The integration of 2D computer vision constraints with 3D reconstruction techniques enables increasingly accurate results even from monocular inputs, with recent advances achieving reconstruction times of minutes rather than hours or days, while maintaining high visual quality and animation capabilities.

**Hands:** Human hands are another typical articulated structure that plays a crucial role in everyday life. Similar to the SMPL body model, MANO [34] represents hand geometry with a pre-defined skeleton, blend shapes, and models hand motion using pose parameters and skinning weights. While MANO provides a widely-used parametric foundation, its relatively coarse mesh has led to developments like MANO-HD [125], which offers high-resolution hand geometry while maintaining compatibility with existing MANO-annotated datasets, enabling personalized hand shape fitting using only monocular RGB videos. For realistic hand appearance, researchers have explored diverse representation strategies including neural fields [124, 164], radiance fields [126, 165], and texture maps [166, 167, 168], with methods like RelightableHands [169], HandRT [170], and URHand [168] enabling physically-based relighting through explicit material modeling. Hand reconstruction approaches increasingly address complex interaction scenarios, including hand-to-hand [165, 171] and hand-to-object interactions [172, 173]. Recent advances have introduced novel representations such as LiveHand’s [126] UVH space parameterization that represents hands relative to the MANO surface without explicit skinning, Nimble’s [174] modeling of inner bones and muscles for enhanced biomechanical realism. MANUS [128] effectively represents articulated hands by utilizing 3D Gaussian Splatting in canonical space and employing forward skinning to convert these Gaussians into posed space, where the model is supervised through multi-view sequences to achieve precise shape and appearance reconstruction. GaussianHand [127] enhances articulated hand modeling by leveraging canonical features to refine blend shapes derived from parametric models like MANO and implementing neural residual skeletons to

Method	Venue	Input	Auxiliary				Motion rep.	Obj. rep.
			Prior	Norm	Mask	L.P.		
Human body								
Neural Body [30]	CVPR'21	multi-view	SMPL				forward skinning	voxel grids
A-NeRF [113]	NeurIPS'21	monocular	skeleton			✓	skeleton-relative encoding	MLP
NARF [114]	ICCV'21	monocular	skeleton		✓		forward skinning	part-wise
AN [115]	ICCV'21	multi-view	SMPL				inverse skinning	MLP
NHP [116]	NeurIPS'21	multi-view	SMPL				inverse skinning	p.a. feat.
Vid2Avatar [117]	CVPR'23	casual	skeleton	✓	✓		inverse skinning	MLP
MonoHuman [95]	CVPR'23	monocular	SMPL		✓		bidirectional deformation	MLP
InstantAvatar [95]	CVPR'23	monocular	skeleton		✓		forward skinning	HashGrids
ExAvatar [118]	ECCV'24	casual	SMPL-X	✓	✓	✓	forward skinning	3DGS
HuGS [31]	CVPR'24	monocular	SMPL		✓		forward skinning	3DGS
GART [48]	CVPR'24	monocular	SMPL				forward skinning	3DGS
GauHuman [119]	CVPR'24	monocular	SMPL			✓	forward skinning	3DGS
Animatable Gaussians! [120]	CVPR'24	multi-view	SMPL-X				forward skinning	3DGS
GaussianAvatar [121]	CVPR'24	monocular	SMPL-X			✓	forward skinning	3DGS
ASH [122]	CVPR'24	multi-view	skeleton				DQS	3DGS
MoDA [123]	IJCV'24	casual			✓		NeuDBS	MLP
Hand								
LISA [124]	CVPR'22	multi-view	MANO			✓	inverse skinning	SDF
HandAvatar [125]	CVPR'23	monocular	MANO-HD				forward skinning	Occupancy
LiveHand [126]	ICCV'23	multi-view	MANO				UVH	MLP
GaussianHand [127]	TVCG'24	multi-view	MANO				forward skinning	3DGS
MANUS [128]	CVPR'24	multi-view	skeleton				forward skinning	3DGS
Animal								
ARTEMIS [129]	TOG'22	multi-view	skeleton		✓		forward skinning	voxel grids
BANMo [86]	CVPR'22	casual			✓	✓	forward skinning	MLP
MagicPony [130]	CVPR'23	single view	skeleton		✓		forward skinning	SDF
CoP3D [131]	CVPR'23	casual			✓		trajectory	p.a. feat.
AnimalAvatar [132]	ECCV'24	monocular	SMAL		✓	✓	forward skinning	Triplane
Object								
CLA-NeRF [133]	ICRA'22	multi-view			✓	✓	joint para.	MLP
PARIS [134]	ICCV'23	multi-view			✓		joint para.	HashGrids
LEIA [135]	ECCV'24	multi-view					state code	MLP
REACTO [136]	CVPR'24	casual			✓		QRBS	MLP
ArtGS [137]	ICLR'25	multi-view					SE(3)	3DGS

TABLE 2: Selected papers for dynamic scene reconstruction with articulated motion. L.P. stands for **L**earnable **P**ose.

capture subtle pose-dependent deformations, resulting in more accurate representation of hand poses than methods using only standard linear blend skinning.

**Animal:** Reconstructing articulated animals presents unique challenges due to the vast diversity of species, making it difficult to adapt a single template to accommodate all morphologies. The SMAL model [175], a pioneering parametric 3D representation, focuses primarily on quadruped animals and provides a foundation for subsequent research. Based on this parametric framework, researchers have demonstrated that animal shapes can be accurately fitted using only 2D image inputs [176]. More recently, neural radiance field approaches have enabled learning detailed geometry and appearance [86, 129, 132], allowing for photorealistic novel view synthesis through volume rendering. These methods typically employ a dual-level representation strategy: a category-level template for general morphology combined with instance-level corrections to capture individual variations [87].

Several innovative approaches have moved beyond template meshes, instead using only skeletal structures as priors [129, 130, 177], where the posed animal is driven entirely by skeletal motion. Even more remarkably, some methods operate without any species-specific prior knowledge, learn-

ing animal models automatically from raw data [86, 131, 178], demonstrating the versatility of articulated motion representations across diverse morphologies. For example, BANMo [86] learns neural bones and skinning weights directly from casual videos, representing animals as density and color radiance fields in canonical space, with point correspondences established through bidirectional neural skinning operations. ARTEMIS [129] represents geometry and appearance using neural radiance feature voxel grids, with posed animals warped via skeletal motion and rendered through neural rendering techniques. CoP3D [131] utilizes pixel-aligned features to estimate density and color without explicitly modeling motion. Learning the articulation from casually monocular videos remains an inherently ill-posed problem, these methods leverage various auxiliary information sources to constrain the solution space, including foreground masks [129, 132], optical flow [86, 131], surface normals [87], and semantically rich features from foundation models such as CSE [132] and DINO [177].

**Objects:** Unlike human or animal bodies with consistent skeletal structures, general articulated objects (such as laptops, scissors, and other mechanical devices) present unique reconstruction challenges due to their diverse topologies and joint configurations. For these objects, using pre-defined

kinematic trees becomes impractical, as each object type features distinct articulation patterns. The key challenge in reconstructing such general articulated objects involves three interrelated tasks: accurately segmenting the constituent parts, defining appropriate joint motion types (e.g., rotational, prismatic), and estimating precise joint motion parameters for each articulated state [179].

Recent advances in neural radiance field techniques have enabled significant progress in part-level geometry and appearance reconstruction combined with joint motion parameter estimation [133, 134, 137]. Several approaches address this challenge from different perspectives. PARIS [134] simplifies the problem by assuming objects contain only one movable part and represents articulated motion through explicit joint motion parameters, storing geometry and appearance in efficient Instant-NGP-style hash grids [4]. Taking a different approach, CLA-NeRF [133] employs category-level semantic neural radiance fields to segment individual parts and represents the motion between each part and a designated root part through rigid transformations. Rather than directly modeling joint motions, LEIA [135] introduces a more abstract approach using latent state codes to represent different articulation states. REACTO [136] offers a more flexible solution by implementing Quasi-Rigid Blend Skinning (QRBS) to represent articulation motion, learning neural bones and skinning weights directly from casually captured monocular video without requiring explicit part segmentation or predefined articulation models.

### 4.3 Reconstructing with Non-rigid Motion

**4D Spacetime.** A complete light field is traditionally represented as a 7D plenoptic function  $f(\mathbf{x}, \mathbf{d}, \lambda, t)$  [190], which simplifies to a 5D function for static scenes by removing time and wavelength dependencies. For dynamic scenes, researchers reintroduce time  $t$ , creating a 6D plenoptic function that models the scene as a continuous 4D spatiotemporal volume [26, 91]. This unified representation implicitly encodes scene geometry, appearance, and motion within the same field structure, with properties like density and color varying temporally without explicitly modeling motion vectors. To enhance efficiency and visual fidelity, recent methods decompose scenes into time-invariant static backgrounds (5D) and time-dependent [94, 180] or latent code conditioned [41] dynamic foregrounds (6D), blended via learned weights and often guided by segmentation masks [79, 191] or self-supervised techniques [192]. Implementation approaches have evolved from MLPs to more efficient structures: some methods use 4D neural voxels for accelerated rendering [90, 193, 194], while others leverage 3D Gaussian splatting to model 4D spacetime as sequential slices of 3D space with time-dependent Gaussian properties [27, 181], enabling real-time rendering of complex non-rigid motion while maintaining temporal consistency.

**Canonical Space with Deformation Field.** In contrast to frame-by-frame 4D spacetime optimization that entangles motion and scene representation within a single radiance field, an alternative approach decomposes dynamic scenes into a static reference volume (canonical space) and its temporal evolution pattern (deformation field). The canonical space serves as a consistent template representation,

while the deformation field describes how each point moves across time. For structured subjects like human bodies or faces, the canonical space often represents a neutral pose or expression. For general scenes, it typically corresponds to the scene configuration at an initial time point  $t_0$ .

In neural radiance field implementations, this approach typically employs backward deformation—points sampled along camera rays in the observation space are transformed back to canonical space through the deformation field, as their density and color properties are stored in the canonical representation. In contrast, explicit representations like 3D Gaussian fields can directly apply forward deformation, warping each Gaussian primitive from canonical to observation space. Neither approach alone guarantees perfect consistency between spaces, leading some methods to implement bijective deformation fields that maintain correspondences in both directions.

For extended sequences with substantial motion or appearance changes, a single global canonical space often proves insufficient. In such cases, multiple local canonical spaces (keyframes) shared by temporal subwindows provide a more effective solution [184]. This approach allows nearby frames to reference the same canonical space while temporally distant frames leverage different reference volumes, better accommodating dramatic transformations while maintaining local consistency.

**Frame-to-Frame Flow Field.** An alternative approach to representing dynamic scenes involves modeling motion as point correspondences between consecutive frames, known as frame-to-frame motion fields or scene flow fields. These fields typically formulate the motion relationship between adjacent frames, where smaller displacements make the motion patterns easier to learn and model. This flow field is generally implemented as a 4D function that maps 3D spatial positions and a 1D time parameter to corresponding displacement vectors [37, 38, 195].

Rather than representing flow in only one direction, bidirectional approaches enhance reconstruction quality. For example, Li et al. [13] utilize both forward and backward flow fields within the same framework, establishing point correspondences between frames  $i$  and  $j$  along rays. When points from frame  $i$  move to frame  $j$  along flow field  $f_{i \rightarrow j}$ , the rendered results should maintain consistency with frame  $j$ , and vice versa. This bidirectional consistency effectively enables information sharing between adjacent frames, serving as a powerful constraint that enhances learning efficiency [96].

The framework can be extended by transferring points from a target frame to multiple source frames, allowing information aggregation across temporal neighbors for more generalizable and adaptive reconstructions [131, 185, 186]. Since scene flow fields naturally exhibit non-zero values only in dynamic regions, decomposing scenes into static and dynamic components significantly benefits the learning of meaningful flow fields [13, 37, 185, 186, 195].

Beyond direct flow field learning, an alternative formulation treats flow fields as the integration of velocity fields over time [19, 19, 38, 96]. While flow fields are typically constrained by smoothness and continuity regularizations, velocity fields offer additional physical constraints and directional information through their vector nature. Li et

Method	Venue	Input	Auxiliary				Motion rep.	Obj. rep.
			Depth	Mask	O.F.	Reg.		
4D Spacetime								
Neural Volumes [91]	ToG'19	multi-view		✓		TV	latent code	RGBA volume
VideoNeRF [26]	CVPR'21	casual	✓			CE	time	MLP
DyNeRF [41]	CVPR'22	multi-view					latent code	MLP
D <sup>2</sup> NeRF [92]	NeurIPS'22	monocular				CE	latent code	MLP
TiNeuVox [39]	SIGGRAPH Asia'22	multi-view				CE	time	voxel grids
NeRFPlayer [40]	TVCG'23	monocular				CE	time	voxel grids
SUDS [79]	CVPR'23	monocular	✓		✓	CE/cycle	frame index	HashGrids
MLP Maps [180]	CVPR'23	multi-view					latent code	factorized planes
4DGS [27]	ICLR'24	monocular					time	3DGS
STG [181]	CVPR'24	multi-view					time	gaussian feature
GFlow [182]	AAAI'25	monocular	✓		✓		time	3DGS
Canonical Space with Deformation Field								
Nerfies [9]	ICCV'21	multi-view		✓		elastic	latent code	MLP
D-NeRF [8]	CVPR'21	monocular					time	MLP
HyperNeRF [10]	TOG'21	casual					latent code	MLP
NDVG [183]	ACCV'22	monocular		✓		CE/TV/ $L_1$	time	MLP
HyperReel [184]	CVPR'23	multi-view					velocity	factorized planes
GauFRe [43]	Arxiv'23	monocular					time	3DGS
Deformable 3DGS [12]	CVPR'24	monocular					time	3DGS
MoDGS [93]	Arxiv'24	casual	✓		✓		time	3DGS
GA-GS [44]	CVPR'24	monocular				$L_1$	time	3DGS
Frame-to-Frame Flow Field								
NeRFlow [38]	ICCV'21	monocular					flow field	MLP
DynamicNeRF [37]	ICCV'21	monocular	✓	✓	✓	CE/TV/cycle/ $L_1$	scene flow	MLP
NSFF [13]	CVPR'21	multi-view	✓	✓	✓	cycle/ $L_1$	scene flow	MLP
MonoNeRF [185]	ICCV'23	monocular	✓	✓	✓	cycle	velocity field	MLP
FSDNeRF [19]	CVPR'23	monocular		✓	✓		velocity field	MLP
DynPoint [186]	NeurIPS'24	Monocular	✓	✓	✓		scene flow	neural points
Point Tracking								
DCT-NeRF [23]	Arxiv'21	monocular	✓		✓	TV/ARAP/cycle/ $L_1$	trajectory	MLP
PVG [46]	Arxiv'23	monocular	✓	✓		$L_1$	trajectory	3DGS
OmniMotion [18]	ICCV'23	monocular			✓	cycle/ $L_1$	bijjective mapping	MLP
DynGS [17]	3DV'24	multi-view		✓		ARAP/isometric	time	3DGS
Marbles [45]	SIGGRAPH Asia'24	casual		✓		isometric	trajectory	3DGS
Factorization								
NPGs [187]	CVPR'24	monocular		✓	✓	isometric	basis	3DGS
FPO [188]	CVPR'22	multi-view		✓			basis	voxel grids
Tensor4D [42]	CVPR'23	multi-view				TV	feature planes	MLP
Hexplane [15]	CVPR'23	monocular				TV	feature planes	MLP
K-Planes [14]	CVPR'23	monocular				TV/Laplacian/ $L_1$	feature planes	MLP
4K4D [152]	CVPR'24	multi-view		✓			feature planes	MLP
4D GS [11]	CVPR'24	monocular				TV	feature planes	3DGS
DeformGS [47]	WAFR'24	multi-view		✓		isometric	feature planes	3DGS
DynMF [189]	ECCV'24	monocular				isometric/ $L_1$	basis	3DGS

TABLE 3: Selected papers for dynamic scene reconstruction with non-rigid motion.

al. [196] demonstrate this by incorporating physical laws as supervision through physics-informed neural networks (PINNs), enabling applications like future frame extrapolation, motion transfer, and semantic decomposition. Regardless of whether flow fields or velocity fields are employed, 2D optical flow provides valuable supervision signals for learning [13, 38, 185, 186], particularly in monocular settings where depth information is limited.

**Point Tracking:** Traditional approaches to dynamic scene reconstruction employ either canonical spaces with deformation fields or frame-to-frame progressive evolution. Both methods calculate point correspondences indirectly through proxy spaces (canonical or reference frames), which becomes problematic for long-term correspondence as errors accumulate along transformation chains.

An effective alternative models each point's movement as a continuous trajectory, a time-dependent function that directly describes position at any moment in the continuous spacetime domain [23, 181]. This global trajectory formulation represents the complete motion path as a unified function, eliminating cascading errors from sequential transformations. With this approach, a point's geometry and appearance can be modeled as time-varying radiance properties while maintaining temporal consistency [18].

For multi-view capture scenarios, 3D Gaussian Splatting methods can initialize the scene representation from the first frame and subsequently track each Gaussian primitive's movement through space over time [17, 45]. This tracking approach can maintain consistent appearance properties (density and color) while updating positions, providing a

Method	Venue	Input	Auxiliary				Motion rep.	Obj. rep.
			Prior	O.F.	Mask	Depth		
NA [36]	TOG'21	multi-view	SMPL				inverse skinning+deformation	MLP
NeuMan [141]	ECCV'22	monocular	SMPL		✓		inverse skinning+deformation	MLP
HumanNeRF [35]	CVPR'22	casual	skeleton		✓		inverse skinning+deformation	MLP
TAVA [84]	ECCV'22	multi-view	skeleton				skinning+deformation	MLP
Instant-NVR [159]	CVPR'23	monocular	SMPL				inverse skinning+deformation	part-wise
HandNeRF [165]	CVPR'23	multi-view	MANO		✓		inverse skinning+deformation	MLP
HOSNeRF [197]	CVPR'23	monocular	skeleton	✓	✓		inverse skinning+deformation	MLP
ExAvatar [118]	ECCV'24	casual	SMPL-X		✓		skinning+deformation	3DGS
GoMAvatar [157]	CVPR'24	monocular	SMPL		✓		skinning+deformation	3DGS
3DGS-Avatar [49]	CVPR'24	monocular	SMPL		✓		skinning+deformation	3DGS
OmniRe [80]	ICLR'25	multi-view	6DoF		✓	✓	rigid+articulated+non-rigid	3DGS

TABLE 4: Selected papers for dynamic scene reconstruction with hybrid motion.

more robust foundation for dynamic scene reconstruction with greater temporal coherence.

**Factorization:** The concept of factorization for radiance fields emerged from static scene reconstruction, where methods like TensorRF [5] decompose 3D space into low-rank 1D vectors or 2D matrices to improve computational and memory efficiency. This approach has been successfully extended to 4D dynamic scenes through spatiotemporal factorization.

Hexplane [15] decomposes the 4D domain into six feature planes, where point features are sampled via interpolation and concatenated to predict density and color. Similarly, K-planes [14] offers a unified approach for both static and dynamic scenes—factorizing static 3D space into  $xy, yz, xz$  planes while representing dynamic 4D spacetime with  $xt, yt, zt$  planes, incorporating multi-scale sampling for enhanced representation. This efficient spatiotemporal factorization enables higher grid resolution and rapid convergence, making it a foundation for numerous subsequent methods [42, 198, 199, 200]. For instance, 4K4D [152] extends K-plane’s 4D feature grid factorization to achieve real-time performance at 4K resolution, while Wu et al. [11] use factorized spatiotemporal structures to encode per-Gaussian features for deformation field decoding.

Beyond basic spatiotemporal factorization, motion fields can also be factorized into a compact set of basis functions. This approach represents complex motion using a few representative spatial deformation patterns, enhancing temporal coherence while improving learning stability and storage efficiency. Li et al. [20] model the motion field as spatially decomposed motion bases with time-varying coefficients, using pixel-aligned features sampled from source to target views and fused by a ray transformer. While some methods represent both motion bases and coefficients as learnable neural network parameters [201, 202], others leverage sinusoidal bases [23, 188, 203].

For Gaussian-based representations, Kratimenos et al. [189] factorize 3D Gaussian motion into a small number of motion bases—significantly fewer than the number of Gaussian primitives—with regularization applied to the motion coefficients to ensure plausible movements. Das et al. [187] propose a two-stage approach: first learning a coarse proxy using factorized motion bases and low-rank coefficients, then initializing local volumes with 3D Gaussians refined through adaptive densification. The shared motion bases in the coarse stage force information sharing

between timesteps, providing essential regularization for sparsely observed dynamic regions.

#### 4.4 Reconstructing with Hybrid Motion

Dynamic objects in real-life scenarios often exhibit complex motion patterns that combine rigid, articulated, and non-rigid components. In autonomous driving scenes, for example, vehicles primarily undergo rigid motion, while pedestrians and cyclists move in more complex, non-rigid ways. To address this diversity, Fischer et al [51] leveraged tracking results with bounding boxes to represent rigid vehicles while employing non-rigid motion fields to model other dynamic objects. Taking a more comprehensive approach, OmniRe [80] developed a framework that combines distinct motion representations within a dynamic scene graph: rigid nodes for vehicles, SMPL nodes for articulated pedestrian motion, and deformable nodes for general non-rigid objects—creating a unified framework for urban scene reconstruction.

Human avatar reconstruction presents another challenging hybrid motion scenario, particularly when modeling dynamic elements like hair and clothing alongside the articulated human body. Generally, there are two primary strategies for combining non-rigid deformation with articulated skinning motion. The first approach operates in canonical space, where points from observation space are initially transformed via inverse skinning, and then non-rigid deformation is applied within the canonical space [35, 36, 141, 165]. The alternative approach works in observation space, first transforming the canonical body to observation space through forward skinning, then applying non-rigid displacement under the target pose [84, 118, 157]. These deformation fields typically take encoded time stamps or pose parameters as inputs to the neural networks, allowing them to capture time- and pose-dependent displacements effectively. In MonoHuman [95], a hybrid approach combines forward and inverse skinning motions with two separate non-rigid deformation fields, representing the non-rigid displacements both in target and observation space.

#### 4.5 Auxiliary Information and Regularization

##### 4.5.1 Auxiliary Information

**Depth Information** serves as a crucial geometric cue for 3D scene reconstruction, particularly valuable in dynamic

scenarios where it helps mitigate ambiguities in scale, motion, and geometry. This spatial information can be acquired through various approaches, ranging from direct sensor measurements via RGB-D cameras or LiDAR systems to algorithmic estimation techniques. In neural radiance fields, depth is rendered by replacing the color value in the volume rendering equation (Eq. 3), while in 3D Gaussian splatting, depth is obtained by rasterizing the Gaussian positions during splatting (Eq. 4). Through gradient backpropagation, supervising the rendered depth in observation space significantly aids the learning of both radiance fields and motion fields [94, 204], particularly beneficial in challenging outdoor environments [106, 107, 108, 111]. When dedicated depth sensors are unavailable, monocular depth estimation methods [205, 206] can provide valuable geometric cues despite scale ambiguity [16, 93, 182, 204]. Beyond providing additional geometric supervision, depth information enables importance sampling in regions near object surface, substantially reducing unnecessary computational overhead in volume-based rendering methods [79, 207].

**Surface Normals** capture fine-grained geometric details that might be missed in continuous and smooth neural representations, making them valuable for high-fidelity reconstruction. In dynamic scenes, surface normals are particularly useful in tracking shape deformations [85, 157] and modeling view-dependent reflections [208]. Recent research has successfully leveraged normal information to recover detailed human surface geometry [209, 210, 211], and enhance scene reconstruction [212, 213]. Surface normals are computationally convenient to obtain through automatic differentiation frameworks like PyTorch and TensorFlow, where they can be calculated by differentiating depth with respect to spatial coordinates in volume rendering approaches [117, 214]. In 3D Gaussian splatting, normals can be rendered by taking the direction of the shortest axis of the anisotropic Gaussians [157]. For supervision purposes, pseudo ground truth normals can be derived by being directly estimated via foundation models like Metric3D [215] or calculated from template meshes [36, 159, 167].

**Semantic Information** serves as a powerful auxiliary cue for dynamic scene reconstruction, enabling more nuanced understanding and accurate modeling of moving objects. In dynamic scenes, object-level semantic segmentation provides valuable silhouettes or foreground masks that help localize dynamic objects and decompose scenes into static backgrounds and dynamic foregrounds [94, 208, 216]. This semantic decomposition is particularly valuable for complex urban environments and scenes with multiple moving entities [22, 106]. Beyond object-level segmentation, part-level semantic information recognizes the rigid components of articulated objects [217], enforcing part consistency throughout the dynamic reconstruction process and enabling more detailed part-wise reconstruction [218]. At the finest granularity, pixel-level semantic features facilitate robust point tracking and establish reliable correspondences across frames [131, 132, 186, 219, 220], which is essential for tracking deformations and understanding complex motion patterns.

**Data-driven Priors** significantly enhance dynamic scene reconstruction by leveraging implicit knowledge from large-scale datasets to provide valuable constraints during opti-

mization. Foundation models trained on diverse data deliver robust priors across multiple modalities, including Depth Anything [206] for monocular depth estimation, Metric3D [215] for surface normals, and Segment Anything [221] for semantic segmentation—all serving as effective supervision signals without specialized sensors. For motion understanding, optical flow models like UniMatch [222] establish dense correspondences between frames [86, 161, 162, 223], while object tracking models generate reliable trajectories for rigid objects and statistical parametric models such as SMPL [33] and SMPL-X [82] encode strong priors about human body shape and pose. Additionally, visual foundation models like DINO [104] extract semantic features that maintain consistency across different viewpoints and lighting conditions, providing robust cues for establishing correspondences in challenging scenarios [130, 165, 177, 195], ultimately improving reconstruction quality in situations with sparse views, fast motion, or challenging lighting.

#### 4.5.2 Regularization

In real-world scenarios, object motion exhibits continuity—neighboring points tend to move similarly, and trajectories evolve gradually over time. To enforce this smoothness mathematically, Total Variation (TV) loss encourages motion fields  $f$  to be piecewise constant, creating natural transitions between differently moving regions [14, 91, 224]:

$$\mathcal{L}_{TV} = \sum_{i,j} |f(i+1, j) - f(i, j)| + |f(i, j+1) - f(i, j)|. \quad (24)$$

Complementing TV loss, Laplacian loss penalizes sharp gradient changes, ensuring smoother transitions in deformation fields by operating on second-order derivatives [153].

Beyond smoothness, maintaining the physical structure of objects during deformation is crucial for realism. The As-Rigid-As-Possible (ARAP) constraint preserves local structural integrity by maintaining relative distances between neighboring points. This approach is particularly effective for short-term local rigidity, ensuring that each small neighborhood deforms as rigidly as possible. While ARAP focuses on local rigidity, isometric loss ensures global structural consistency by preserving geodesic distances across the entire shape:

$$\mathcal{L}_{iso} = \sum_{i=1}^{N_p} \sum_{j \in \mathcal{N}_k(i)} \|d(\mathbf{x}_i, \mathbf{x}_j) - d(\mathbf{x}_i^t, \mathbf{x}_j^t)\|_1, \quad (25)$$

In addition to these, the divergence loss encourages volume preservation by constraining deformation fields to primarily consist of translations and rotations. This property is critical for realistic modeling of real-world object deformations where material volume typically remains constant during movement.

Besides these physical constraints, scene priors contribute significantly to guiding reconstruction. For example, applying  $L_1$  regularization on motion fields biases the scene toward static components—a reasonable assumption given that dynamic objects typically occupy only a small portion of the scene [26, 192]. This regularization not only favors a mostly static background but also facilitates a more robust static-dynamic decomposition during analysis. Moreover, cycle consistency constraints play a critical role

in verifying reconstruction accuracy. By enforcing consistent correspondences between features, motions, or colors across frames, these constraints help maintain temporal coherence [13, 38, 195]. However, proper handling of occlusions is crucial here, as consistency can only be enforced for points that remain visible in multiple frames. Finally, for volumetric radiance field representations, opacity regularization is employed to promote binary outcomes (0 or 1). This approach mitigates artifacts such as floating regions by reinforcing the assumption that, in most cases, objects are either fully opaque or absent [26, 192].

Together, these complementary regularization strategies guide the optimization process, ensuring that the resulting dynamic scene reconstructions are physically accurate, temporally consistent, and visually plausible.

## 4.6 Discussion

Dynamic scene reconstruction presents significant challenges due to its inherently ambiguous nature, particularly when limited observations are available in monocular settings. These challenges have led to the development of various representation paradigms, each offering different trade-offs between accuracy, efficiency, and flexibility. For rigid objects, the key challenge lies in accurately aligning tracking results from different time stamps into a unified local coordinate system, enabling effective temporal information aggregation. The precision of object localization and tracking therefore becomes fundamental to successful rigid motion reconstruction. While articulated objects consist of rigidly moving parts, their overall motion is non-rigid, making part-level representation more appropriate than object-level approaches. To unify these parts coherently, category-level hierarchical structures are often introduced as priors with specific kinematic constraints. However, developing such kinematic templates is labor-intensive, resulting in templates for only a limited number of articulated motion categories (e.g., humans, quadruped animals). Consequently, template-free reconstruction of articulated motion remains a meaningful yet challenging research direction, with existing approaches showing promise but requiring further quality improvements.

The canonical space approach represents a fundamental design choice where appearance and geometry remain static in a universal reference frame, while neural deformation fields map points between this canonical frame and observed frames. This approach enables effective scene editing with changes propagating through the deformation field, but struggles with sequences exhibiting extreme deformations or topological changes, where maintaining a single coherent canonical space becomes increasingly difficult. Multiple keyframe approaches offer a middle ground by establishing several reference frames rather than relying on a single canonical space. This paradigm relaxes the constraint of finding one universal reference while maintaining temporal coherence across subsets of frames. The extreme case is frame-by-frame optimization in 4D spacetime representation, where each frame functions as its own keyframe. While this approach can achieve high-quality individual frame reconstructions by focusing on per-frame accuracy, it fails to disentangle motion from scene representation,

significantly limiting subsequent manipulation capabilities and producing temporally inconsistent results.

Frame-to-frame flow fields bridge adjacent frames through small point displacements, effectively decomposing complex global deformations into more manageable local transformations. This approach eliminates the need for a shared canonical space and handles large deformations by breaking them into incremental steps. However, these local correspondences often lack temporal consistency over long-term sequences as small errors accumulate over time. Point tracking via trajectory fields addresses this limitation by modeling each point’s path as a continuous function of time rather than discrete connections, constraining motion across an object’s entire lifespan and maintaining temporal coherence throughout the video sequence. However, unrestricted trajectory functions may still yield physically implausible motions without proper regularization.

Motion factorization methods decompose complex motion into a limited set of basis trajectories with time-dependent coefficients, effectively capturing shared motion patterns while reducing the solution search space. This transforms the challenging problem of regularizing implicit motion fields into the more intuitive task of regularizing motion coefficients, often leading to more reasonable and physically plausible recovering. In practical applications, hybrid approaches combining multiple representation paradigms yield superior results, particularly for scenes with mixed motion types including rigid objects, articulated entities, and general non-rigid deformations. The learning paradigm also significantly impacts reconstruction quality, with progressive learning strategies—starting from coarse to fine details, incrementally increasing frequency bands, or employing two-stage reconstruction that separates static and dynamic elements—proving effective in handling complex dynamic scenes while avoiding local minima during optimization.

## 5 CHALLENGES AND FUTURE TRENDS

Considering the advances discussed, we identify several crucial directions for future research that may have broader impact in this field.

### 5.1 Efficient and Robust Reconstruction

Neural radiance fields can render photo-realistic views with impressive quality and compact representation, but suffer from high computational costs during training and inference. While 3D Gaussian splatting achieves real-time performance for static scenes with high quality, the modeling of dynamic motion and time-varying geometry remains time-consuming. Developing efficient reconstruction methods for motion, geometry, and appearance simultaneously is a worthy research direction. For casually captured in the wild videos, camera information is typically unavailable, making robust reconstruction under these challenging conditions practically important. Recent advances in directly regressing 3D point maps from 2D image pairs without camera poses have shown promise for static scenes [225, 226], but adaptation to dynamic environments remains underexplored.

## 5.2 Manipulability and Editability

Manipulation and editing of 2D images and 3D static scenes have seen tremendous progress in recent years. Some methods have attempted to manipulate 4D spacetime representations through scene-level style transfer [227, 228] and object-level operations (removal, addition, repositioning) [106, 107], or by decomposing scenes into static and dynamic regions [229, 230]. However, fine-grained part and pixel-level editing remains challenging. The key to achieving such granularity is accurate point correspondence to propagate edits along the timeline, ensuring temporal consistency. The explicit nature of 3D Gaussian splatting has drawn researchers’ attention to dense tracking [17], showing a potential ability for pixel-level manipulation; however, transforming the unstructured primitives of Gaussian fields into organized hierarchical representations for structured editing of geometry and appearance for general objects still needs significant research attention.

## 5.3 Scalability

Dynamic scenes can be conceptualized as static environments with time-varying motion fields, yet neither component scales effectively across spatial, temporal, or motion dimensions. Spatially, while neural radiance fields offer compact representation with small memory footprints, they struggle when extended to vast environments like urban-scale scenes. Common solutions employ divide-and-conquer strategies [231, 232, 233], but memory costs increase dramatically with scene size, quickly exceeding available GPU memory. Temporally, current methods typically process sequences spanning only seconds or minutes [38, 234], as extending to hours or days becomes computationally prohibitive due to the linear relationship between scene duration and resource requirements. Motion-wise, achieving stable and accurate long-term dense tracking remains challenging due to occlusions, and dramatic changes in object geometry and appearance over time [235]. Despite recent advances like NeVRF [236] and LVV [237], reconstructing large-scale long-term dynamic scenes with complex motions still demands substantial research breakthroughs in unified representations that can simultaneously address spatial extent, temporal duration, and motion complexity constraints.

## 5.4 Reconstruction by Generation

High-quality, comprehensive observations are crucial for dynamic scene reconstruction, yet practical applications typically rely on casually captured monocular data that provides extremely limited visual information, resulting in incomplete reconstructions [75]. While static scene reconstruction has benefited from generative approaches that synthesize invisible or occluded parts using models like LDMs [238], integrating such generative capabilities into 4D dynamic scene reconstruction remains challenging. This integration requires simultaneously maintaining spatial view consistency, temporal coherence, and plausible motion dynamics—a complex multi-constraint problem. Despite recent advances in unconditional, image-based, and text-prompted 4D content generation [239, 240, 241], current methods predominantly output 2D frame sequences without underlying 3D structure [242], thereby failing to provide

comprehensive scene representations. The field now faces the critical challenge of effectively conditioning generative models on monocular or sparse multi-view inputs to produce geometrically and temporally consistent 4D volumetric representations that support free-viewpoint rendering and novel trajectory synthesis.

## 5.5 Large Language Models

Large Language Models (LLMs) [243] offer powerful semantic priors for dynamic scene understanding [244, 245], complementing visual foundation models through their world knowledge and reasoning capabilities. Despite their potential, integrating LLMs with 4D reconstruction presents significant challenges: high-fidelity reconstruction requires pixel-precise geometry and appearance modeling, while LLMs primarily provide high-level semantic abstractions difficult to align with fine-grained visual features. Recent approaches like Language Embedded 3D Gaussians [246, 247] demonstrate promising directions by incorporating quantized semantic features into explicit scene representations, enabling language-guided editing and querying of 3D content. Future research opportunities lie in developing bidirectional interfaces between LLMs’ symbolic reasoning and the continuous spatiotemporal representations required for dynamic scenes, potentially enabling physics-aware and semantically meaningful scene manipulation and generation.

## 6 CONCLUSION AND OUTLOOK

In this survey, we present a comprehensive overview of dynamic motion and scene representation in radiance fields, focusing on Neural Radiance Fields and 3D Gaussian Splatting. By systematically categorizing motion into rigid, articulated, non-rigid, and hybrid types, we analyze diverse approaches across the literature, highlighting their strengths and limitations while identifying critical challenges and promising research directions.

**Outlook.** While 3D scene reconstruction has achieved remarkable success, the research frontier has shifted toward comprehensive 4D dynamic volume reconstruction—the cornerstone of world models. Powered by advances in neural rendering, generative models, foundation models, and LLMs, we anticipate rapid progress in simultaneously addressing two fundamental challenges: photorealistic geometry and appearance reconstruction, and consistent, physically plausible temporal motion recovering. In summary, 4D dynamic scene reconstruction presents both significant opportunities and challenges, with the ultimate goal of creating high-fidelity digital twins of real dynamic physical environments. In this era of emerging technologies, we hope this survey serves as a valuable foundation to inspire researchers pursuing advances in this transformative domain.

## ACKNOWLEDGMENTS

This project is partially supported by NSFC (62476075 and 62376080), the Zhejiang Provincial Natural Science Foundation Key Fund of China (LZ23F030003), and the Zhejiang Province Key Laboratory of Optoelectronic Intelligent Imaging and Aerospace Sensing.

## REFERENCES

- [1] B. Mildenhall, P. P. Srinivasan, M. Tancik, J. T. Barron, R. Ramamoorthi, and R. Ng, "Nerf: Representing scenes as neural radiance fields for view synthesis," *Commun. ACM*, vol. 65, no. 1, pp. 99–106, 2021.
- [2] B. Kerbl, G. Kopanas, T. Leimkühler, and G. Drettakis, "3d gaussian splatting for real-time radiance field rendering," *ACM TOG*, vol. 42, July 2023.
- [3] M. Niemeyer, L. Mescheder, M. Oechsle, and A. Geiger, "Differentiable volumetric rendering: Learning implicit 3d representations without 3d supervision," in *CVPR*, pp. 3504–3515, 2020.
- [4] T. Müller, A. Evans, C. Schied, and A. Keller, "Instant neural graphics primitives with a multiresolution hash encoding," *ACM TOG*, vol. 41, no. 4, pp. 1–15, 2022.
- [5] A. Chen, Z. Xu, A. Geiger, J. Yu, and H. Su, "Tensorf: Tensorial radiance fields," in *ECCV*, pp. 333–350, Springer, 2022.
- [6] J. T. Barron, B. Mildenhall, M. Tancik, P. Hedman, R. Martin-Brualla, and P. P. Srinivasan, "Mip-nerf: A multiscale representation for anti-aliasing neural radiance fields," in *ICCV*, pp. 5855–5864, 2021.
- [7] Z. Yu, A. Chen, B. Huang, T. Sattler, and A. Geiger, "Mip-splatting: Alias-free 3d gaussian splatting," in *CVPR*, pp. 19447–19456, 2024.
- [8] A. Pumarola, E. Corona, G. Pons-Moll, and F. Moreno-Noguer, "D-nerf: Neural radiance fields for dynamic scenes," in *CVPR*, pp. 10318–10327, 2021.
- [9] K. Park, U. Sinha, J. T. Barron, S. Bouaziz, D. B. Goldman, S. M. Seitz, and R. Martin-Brualla, "Nerfies: Deformable neural radiance fields," in *ICCV*, pp. 5865–5874, 2021.
- [10] K. Park, U. Sinha, P. Hedman, J. T. Barron, S. Bouaziz, D. B. Goldman, R. Martin-Brualla, and S. M. Seitz, "Hypernerf: a higher-dimensional representation for topologically varying neural radiance fields," *ACM TOG*, vol. 40, no. 6, pp. 1–12, 2021.
- [11] G. Wu, T. Yi, J. Fang, L. Xie, X. Zhang, W. Wei, W. Liu, Q. Tian, and X. Wang, "4d gaussian splatting for real-time dynamic scene rendering," in *CVPR*, pp. 20310–20320, 2024.
- [12] Z. Yang, X. Gao, W. Zhou, S. Jiao, Y. Zhang, and X. Jin, "Deformable 3d gaussians for high-fidelity monocular dynamic scene reconstruction," in *CVPR*, pp. 20331–20341, 2024.
- [13] Z. Li, S. Niklaus, N. Snavely, and O. Wang, "Neural scene flow fields for space-time view synthesis of dynamic scenes," in *CVPR*, pp. 6498–6508, 2021.
- [14] S. Fridovich-Keil, G. Meanti, F. R. Warburg, B. Recht, and A. Kanazawa, "K-planes: Explicit radiance fields in space, time, and appearance," in *CVPR*, pp. 12479–12488, 2023.
- [15] A. Cao and J. Johnson, "Hexplane: A fast representation for dynamic scenes," in *CVPR*, pp. 130–141, 2023.
- [16] Y.-L. Liu, C. Gao, A. Meuleman, H.-Y. Tseng, A. Saraf, C. Kim, Y.-Y. Chuang, J. Kopf, and J.-B. Huang, "Robust dynamic radiance fields," in *CVPR*, pp. 13–23, 2023.
- [17] J. Luiten, G. Kopanas, B. Leibe, and D. Ramanan, "Dynamic 3d gaussians: Tracking by persistent dynamic view synthesis," in *International Conference on 3D Vision (3DV)*, 2024.
- [18] Q. Wang, Y.-Y. Chang, R. Cai, Z. Li, B. Hariharan, A. Holynski, and N. Snavely, "Tracking everything everywhere all at once," in *ICCV*, pp. 19795–19806, 2023.
- [19] C. Wang, L. E. MacDonald, L. A. Jeni, and S. Lucey, "Flow supervision for deformable nerf," in *CVPR*, pp. 21128–21137, 2023.
- [20] Z. Li, Q. Wang, F. Cole, R. Tucker, and N. Snavely, "Dynibar: Neural dynamic image-based rendering," in *CVPR*, pp. 4273–4284, 2023.
- [21] X. Fu, S. Zhang, T. Chen, Y. Lu, L. Zhu, X. Zhou, A. Geiger, and Y. Liao, "Panoptic nerf: 3d-to-2d label transfer for panoptic urban scene segmentation," in *3DV*, pp. 1–11, 2022.
- [22] A. Kundu, K. Genova, X. Yin, A. Fathi, C. Pantofaru, L. J. Guibas, A. Tagliasacchi, F. Dellaert, and T. Funkhouser, "Panoptic neural fields: A semantic object-aware neural scene representation," in *CVPR*, pp. 12871–12881, 2022.
- [23] C. Wang, B. Eckart, S. Lucey, and O. Gallo, "Neural trajectory fields for dynamic novel view synthesis," *arXiv preprint arXiv:2105.05994*, 2021.
- [24] N. Max, "Optical models for direct volume rendering," *TVCG*, vol. 1, no. 2, pp. 99–108, 1995.
- [25] J. Ost, F. Mannan, N. Thuerey, J. Knodt, and F. Heide, "Neural scene graphs for dynamic scenes," in *CVPR*, pp. 2856–2865, 2021.
- [26] W. Xian, J.-B. Huang, J. Kopf, and C. Kim, "Space-time neural irradiance fields for free-viewpoint video," in *CVPR*, pp. 9421–9431, 2021.
- [27] Z. Yang, H. Yang, Z. Pan, and L. Zhang, "Real-time photorealistic dynamic scene representation and rendering with 4d gaussian splatting," in *The Twelfth ICLR*.
- [28] X. Zhou, Z. Lin, X. Shan, Y. Wang, D. Sun, and M.-H. Yang, "Drivinggaussian: Composite gaussian splatting for surrounding dynamic autonomous driving scenes," in *CVPR*, pp. 21634–21643, 2024.
- [29] M. Zwicker, H. Pfister, J. Van Baar, and M. Gross, "Ewa volume splatting," in *IEEE Visualization 2001*, pp. 29–538, IEEE, 2001.
- [30] S. Peng, Y. Zhang, Y. Xu, Q. Wang, Q. Shuai, H. Bao, and X. Zhou, "Neural body: Implicit neural representations with structured latent codes for novel view synthesis of dynamic humans," in *CVPR*, pp. 9054–9063, 2021.
- [31] M. Kocabas, J.-H. R. Chang, J. Gabriel, O. Tuzel, and A. Ranjan, "Hugs: Human gaussian splats," in *CVPR*, pp. 505–515, 2024.
- [32] W. Yuan, Z. Lv, T. Schmidt, and S. Lovegrove, "Star: Self-supervised tracking and reconstruction of rigid objects in motion with neural rendering," in *CVPR*, pp. 13144–13152, 2021.
- [33] M. Loper, N. Mahmood, J. Romero, G. Pons-Moll, and M. J. Black, "Smpl: A skinned multi-person linear model," *ACM TOG*, vol. 34, no. 6, 2015.
- [34] J. Romero, D. Tzionas, and M. J. Black, "Embodied hands: Modeling and capturing hands and bodies together," *ACM TOG*, vol. 36, no. 6, pp. 1–17, 2017.
- [35] C.-Y. Weng, B. Curless, P. P. Srinivasan, J. T. Barron, and I. Kemelmacher-Shlizerman, "Humannerf: Free-viewpoint rendering of moving people from monocular video," in *CVPR*, pp. 16210–16220, 2022.
- [36] L. Liu, M. Habermann, V. Rudnev, K. Sarkar, J. Gu, and C. Theobalt, "Neural actor: Neural free-view synthesis of human actors with pose control," *ACM TOG*, vol. 40, no. 6, pp. 1–16, 2021.
- [37] C. Gao, A. Saraf, J. Kopf, and J.-B. Huang, "Dynamic view synthesis from dynamic monocular video," in *ICCV*, pp. 5712–5721, 2021.
- [38] Y. Du, Y. Zhang, H.-X. Yu, J. B. Tenenbaum, and J. Wu, "Neural radiance flow for 4d view synthesis and video processing," in *ICCV*, pp. 14304–14314, 2021.
- [39] J. Fang, T. Yi, X. Wang, L. Xie, X. Zhang, W. Liu, M. Nießner, and Q. Tian, "Fast dynamic radiance fields with time-aware neural voxels," in *SIGGRAPH Asia*, pp. 1–9, 2022.
- [40] L. Song, A. Chen, Z. Li, Z. Chen, L. Chen, J. Yuan, Y. Xu, and A. Geiger, "Nerfplayer: A streamable dynamic scene representation with decomposed neural radiance fields," *TVCG*, vol. 29, no. 5, pp. 2732–2742, 2023.
- [41] T. Li, M. Slavcheva, M. Zollhoefer, S. Green, C. Lassner, C. Kim, T. Schmidt, S. Lovegrove, M. Goesele, R. Newcombe, *et al.*, "Neural 3d video synthesis from multi-view

- video," in *CVPR*, pp. 5521–5531, 2022.
- [42] R. Shao, Z. Zheng, H. Tu, B. Liu, H. Zhang, and Y. Liu, "Tensor4d: Efficient neural 4d decomposition for high-fidelity dynamic reconstruction and rendering," in *CVPR*, pp. 16632–16642, 2023.
- [43] Y. Liang, N. Khan, Z. Li, T. Nguyen-Phuoc, D. Lanman, J. Tompkin, and L. Xiao, "Gaufre: Gaussian deformation fields for real-time dynamic novel view synthesis," in *2025 IEEE/CVF Winter Conference on Applications of Computer Vision (WACV)*, pp. 2642–2652, IEEE, 2025.
- [44] Z. Lu, X. Guo, L. Hui, T. Chen, M. Yang, X. Tang, F. Zhu, and Y. Dai, "3d geometry-aware deformable gaussian splatting for dynamic view synthesis," in *CVPR*, pp. 8900–8910, 2024.
- [45] C. Stearns, A. Harley, M. Uy, F. Dubost, F. Tombari, G. Wetzstein, and L. Guibas, "Dynamic gaussian marbles for novel view synthesis of casual monocular videos," in *SIGGRAPH Asia*, pp. 1–11, 2024.
- [46] Y. Chen, C. Gu, J. Jiang, X. Zhu, and L. Zhang, "Periodic vibration gaussian: Dynamic urban scene reconstruction and real-time rendering," *arXiv preprint arXiv:2311.18561*, 2023.
- [47] B. P. Duisterhof, Z. Mandi, Y. Yao, J.-W. Liu, J. Seidenschwarz, M. Z. Shou, D. Ramanan, S. Song, S. Birchfield, B. Wen, *et al.*, "Deformgs: Scene flow in highly deformable scenes for deformable object manipulation," *arXiv preprint arXiv:2312.00583*, 2023.
- [48] J. Lei, Y. Wang, G. Pavlakos, L. Liu, and K. Daniilidis, "Gart: Gaussian articulated template models," in *CVPR*, pp. 19876–19887, 2024.
- [49] Z. Qian, S. Wang, M. Mihajlovic, A. Geiger, and S. Tang, "3dgs-avatar: Animatable avatars via deformable 3d gaussian splatting," in *CVPR*, pp. 5020–5030, 2024.
- [50] H. Zhou, J. Shao, L. Xu, D. Bai, W. Qiu, B. Liu, Y. Wang, A. Geiger, and Y. Liao, "Hugs: Holistic urban 3d scene understanding via gaussian splatting," in *CVPR*, pp. 21336–21345, 2024.
- [51] T. Fischer, J. Kulhanek, S. R. Bulò, L. Porzi, M. Pollefeys, and P. Kotschieder, "Dynamic 3d gaussian fields for urban areas," in *NeurIPS*, 2024.
- [52] Y. Yan, H. Lin, C. Zhou, W. Wang, H. Sun, K. Zhan, X. Lang, X. Zhou, and S. Peng, "Street gaussians: Modeling dynamic urban scenes with gaussian splatting," in *ECCV*, pp. 156–173, 2024.
- [53] H. Kato, D. Beker, M. Morariu, T. Ando, T. Matsuoka, W. Kehl, and A. Gaidon, "Differentiable rendering: A survey," *ArXiv Prepr. ArXiv200612057*, 2020.
- [54] R. Gao and Y. Qi, "A Brief Review on Differentiable Rendering: Recent Advances and Challenges," *Electronics*, vol. 13, p. 3546, Jan. 2024.
- [55] F. Dellaert and L. Yen-Chen, "Neural volume rendering: Nerf and beyond," *ArXiv Prepr. ArXiv210105204*, 2020.
- [56] Y. Xie, T. Takikawa, S. Saito, O. Litany, S. Yan, N. Khan, F. Tombari, J. Tompkin, V. Sitzmann, and S. Sridhar, "Neural fields in visual computing and beyond," in *Comput. Graph. Forum*, vol. 41, pp. 641–676, 2022.
- [57] K. Gao, Y. Gao, H. He, D. Lu, L. Xu, and J. Li, "Nerf: Neural radiance field in 3d vision, a comprehensive review," *ArXiv Prepr. ArXiv221000379*, 2022.
- [58] AKM. Rabby and C. Zhang, "BeyondPixels: A comprehensive review of the evolution of neural radiance fields," *ArXiv Prepr. ArXiv230603000*, 2023.
- [59] A. Mittal, "Neural radiance fields: Past, present, and future," *ArXiv Prepr. ArXiv230410050*, 2023.
- [60] G. Chen and W. Wang, "A survey on 3d gaussian splatting," *CoRR*, 2024.
- [61] T. Wu, Y.-J. Yuan, L.-X. Zhang, J. Yang, Y.-P. Cao, L.-Q. Yan, and L. Gao, "Recent advances in 3d gaussian splatting," *Comput. Vis. Media*, vol. 10, no. 4, pp. 613–642, 2024.
- [62] Y. Bao, T. Ding, J. Huo, Y. Liu, Y. Li, W. Li, Y. Gao, and J. Luo, "3d gaussian splatting: Survey, technologies, challenges, and opportunities," *IEEE Trans. Circuits Syst. Video Technol.*, 2025.
- [63] T.-A.-Q. Nguyen, A. Bourki, M. Macudzinski, A. Brunel, and M. Bennamoun, "Semantically-aware neural radiance fields for visual scene understanding: A comprehensive review," *ArXiv Prepr. ArXiv240211141*, 2024.
- [64] L. He, L. Li, W. Sun, Z. Han, Y. Liu, S. Zheng, J. Wang, and K. Li, "Neural Radiance Field in Autonomous Driving: A Survey," *ArXiv Prepr. ArXiv240413816*, 2024.
- [65] F. Tosi, Y. Zhang, Z. Gong, E. Sandström, S. Mattocchia, M. R. Oswald, and M. Poggi, "How nerfs and 3d gaussian splatting are reshaping slam: A survey," *ArXiv Prepr. ArXiv240213255*, vol. 4, 2024.
- [66] E. Šlapak, E. Pardo, M. Dopiriak, T. Maksymyuk, and J. Gazda, "Neural radiance fields in the industrial and robotics domain: Applications, research opportunities and use cases," *Robot. Comput.-Integr. Manuf.*, vol. 90, p. 102810, 2024.
- [67] G. Wang, L. Pan, S. Peng, S. Liu, C. Xu, Y. Miao, W. Zhan, M. Tomizuka, M. Pollefeys, and H. Wang, "NeRF in robotics: A survey," *ArXiv Prepr. ArXiv240501333*, 2024.
- [68] M. Sun, D. Yang, D. Kou, Y. Jiang, W. Shan, Z. Yan, and L. Zhang, "Human 3d avatar modeling with implicit neural representation: A brief survey," in *ISCPs*, pp. 818–827, 2022.
- [69] Y. Ming, X. Yang, W. Wang, Z. Chen, J. Feng, Y. Xing, and G. Zhang, "Benchmarking neural radiance fields for autonomous robots: An overview," *EAAI*, vol. 140, p. 109685, 2025.
- [70] R. Yunus, J. E. Lenssen, M. Niemeyer, Y. Liao, C. Rupprecht, C. Theobalt, G. Pons-Moll, J.-B. Huang, V. Golyanik, and E. Ilg, "Recent Trends in 3D Reconstruction of General Non-Rigid Scenes," May 2024.
- [71] E. Tretschk, N. Kairanda, M. BR, R. Dabral, A. Kortylewski, B. Egger, M. Habermann, P. Fua, C. Theobalt, and V. Golyanik, "State of the Art in Dense Monocular Non-Rigid 3D Reconstruction," in *CGF*, vol. 42, pp. 485–520, 2023.
- [72] M. Gu, J. Li, Y. Wu, H. Luo, J. Zheng, and X. Bai, "3d human avatar reconstruction with neural fields: A recent survey," *Image and Vision Computing*, vol. 154, p. 105341, 2025.
- [73] J. Liu, M. Savva, and A. Mahdavi-Amiri, "Survey on modeling of human-made articulated objects," in *Computer Graphics Forum*, p. e70092, Wiley Online Library, 2024.
- [74] J. K. Aggarwal and Q. Cai, "Human motion analysis: A review," *Computer vision and image understanding*, vol. 73, no. 3, pp. 428–440, 1999.
- [75] H. Gao, R. Li, S. Tulsiani, B. Russell, and A. Kanazawa, "Monocular dynamic view synthesis: A reality check," *NeurIPS*, vol. 35, pp. 33768–33780, 2022.
- [76] K. Byrszki, M. Mazur, J. Tabor, T. Dziarmaga, M. Kądziołka, D. Baran, and P. Spurek, "Raysplats: Ray tracing based gaussian splatting," *arXiv preprint arXiv:2501.19196*, 2025.
- [77] N. Moenne-Loccoz, A. Mirzaei, O. Perel, R. de Lutio, J. Martinez Esturo, G. State, S. Fidler, N. Sharp, and Z. Gojcic, "3d gaussian ray tracing: Fast tracing of particle scenes," *ACM TOG*, vol. 43, no. 6, pp. 1–19, 2024.
- [78] J. K. Aggarwal, Q. Cai, W. Liao, and B. Sabata, "Articulated and elastic non-rigid motion: A review," in *Proceedings of 1994 IEEE Workshop on Motion of Non-rigid and Articulated Objects*, pp. 2–14, IEEE, 1994.
- [79] H. Turki, J. Y. Zhang, F. Ferroni, and D. Ramanan, "Suds: Scalable urban dynamic scenes," in *CVPR*, pp. 12375–12385, 2023.
- [80] Z. Chen, J. Yang, J. Huang, R. de Lutio, J. M. Esturo,

- B. Ivanovic, O. Litany, Z. Gojcic, S. Fidler, M. Pavone, L. Song, and Y. Wang, "OmniRe: Omni Urban Scene Reconstruction," Aug. 2024.
- [81] B. Allen, B. Curless, and Z. Popović, "The space of human body shapes: reconstruction and parameterization from range scans," *ACM TOG*, vol. 22, no. 3, pp. 587–594, 2003.
- [82] G. Pavlakos, V. Choutas, N. Ghorbani, T. Bolkart, A. A. Osman, D. Tzionas, and M. J. Black, "Expressive body capture: 3d hands, face, and body from a single image," in *CVPR*, pp. 10975–10985, 2019.
- [83] S.-Y. Su, T. Bagautdinov, and H. Rhodin, "Npc: Neural point characters from video," in *ICCV*, pp. 14795–14805, 2023.
- [84] R. Li, J. Tanke, M. Vo, M. Zollhofer, J. Gall, A. Kanazawa, and C. Lassner, "Tava: Template-free animatable volumetric actors," in *ECCV*, 2022.
- [85] S. Prokudin, Q. Ma, M. Raafat, J. Valentin, and S. Tang, "Dynamic point fields," in *ICCV*, pp. 7964–7976, 2023.
- [86] G. Yang, M. Vo, N. Neverova, D. Ramanan, A. Vedaldi, and H. Joo, "Banmo: Building animatable 3d neural models from many casual videos," in *CVPR*, pp. 2863–2873, 2022.
- [87] G. Yang, C. Wang, N. D. Reddy, and D. Ramanan, "Reconstructing animatable categories from videos," in *CVPR*, pp. 16995–17005, 2023.
- [88] L. Qiu, G. Chen, J. Zhou, M. Xu, J. Wang, and X. Han, "Rec-mv: Reconstructing 3d dynamic cloth from monocular videos," in *CVPR*, pp. 4637–4646, 2023.
- [89] B. Jiang, Y. Hong, H. Bao, and J. Zhang, "Selfrecon: Self reconstruction your digital avatar from monocular video," in *CVPR*, pp. 5605–5615, 2022.
- [90] S. Park, M. Son, S. Jang, Y. C. Ahn, J.-Y. Kim, and N. Kang, "Temporal interpolation is all you need for dynamic neural radiance fields," in *CVPR*, pp. 4212–4221, 2023.
- [91] S. Lombardi, T. Simon, J. Saragih, G. Schwartz, A. Lehrmann, and Y. Sheikh, "Neural volumes: Learning dynamic renderable volumes from images," *TOG*, vol. 38, pp. 1–14, Aug. 2019.
- [92] T. Wu, F. Zhong, A. Tagliasacchi, F. Cole, and C. Oztireli, "D<sup>2</sup>NeRF: Self-Supervised Decoupling of Dynamic and Static Objects from a Monocular Video," *NeurIPS*, vol. 35, pp. 32653–32666, 2022.
- [93] Q. Liu, Y. Liu, J. Wang, X. Lv, P. Wang, W. Wang, and J. Hou, "MoDGS: Dynamic Gaussian Splatting from Causally-captured Monocular Videos," *ArXiv Prepr. ArXiv240600434*, 2024.
- [94] H. Cai, W. Feng, X. Feng, Y. Wang, and J. Zhang, "Neural surface reconstruction of dynamic scenes with monocular rgb-d camera," *NeurIPS*, vol. 35, pp. 967–981, 2022.
- [95] Z. Yu, W. Cheng, X. Liu, W. Wu, and K.-Y. Lin, "Mono-human: Animatable human neural field from monocular video," in *CVPR*, pp. 16943–16953, 2023.
- [96] M. Niemeyer, L. Mescheder, M. Oechsle, and A. Geiger, "Occupancy flow: 4d reconstruction by learning particle dynamics," in *ICCV*, pp. 5379–5389, 2019.
- [97] E. Rublee, V. Rabaud, K. Konolige, and G. Bradski, "Orb: An efficient alternative to sift or surf," in *ICCV*, pp. 2564–2571, Ieee, 2011.
- [98] B. D. Lucas and T. Kanade, "An iterative image registration technique with an application to stereo vision," in *IJCAI*, vol. 2, pp. 674–679, 1981.
- [99] D. Sun, X. Yang, M.-Y. Liu, and J. Kautz, "Pwc-net: Cnns for optical flow using pyramid, warping, and cost volume," in *CVPR*, pp. 8934–8943, 2018.
- [100] Z. Teed and J. Deng, "Raft: Recurrent all-pairs field transforms for optical flow," in *ECCV*, pp. 402–419, Springer, 2020.
- [101] P. Sand and S. Teller, "Particle video: Long-range motion estimation using point trajectories," *IJCV*, vol. 80, pp. 72–91, 2008.
- [102] C. Doersch, A. Gupta, L. Markeeva, A. Recasens, L. Smaira, Y. Aytar, J. Carreira, A. Zisserman, and Y. Yang, "Tap-vid: A benchmark for tracking any point in a video," *NeurIPS*, vol. 35, pp. 13610–13626, 2022.
- [103] A. W. Harley, Z. Fang, and K. Fragkiadaki, "Particle video revisited: Tracking through occlusions using point trajectories," in *ECCV*, pp. 59–75, Springer, 2022.
- [104] M. Oquab, T. Darcet, T. Moutakanni, H. Vo, M. Szafraniec, V. Khalidov, P. Fernandez, D. Haziza, F. Massa, A. El-Nouby, *et al.*, "Dinov2: Learning robust visual features without supervision," *Transactions on Machine Learning Research Journal*, pp. 1–31, 2024.
- [105] E. R. Chan, C. Z. Lin, M. A. Chan, K. Nagano, B. Pan, S. De Mello, O. Gallo, L. J. Guibas, J. Tremblay, S. Khamis, *et al.*, "Efficient geometry-aware 3d generative adversarial networks," in *CVPR*, pp. 16123–16133, 2022.
- [106] Z. Wu, T. Liu, L. Luo, Z. Zhong, J. Chen, H. Xiao, C. Hou, H. Lou, Y. Chen, R. Yang, *et al.*, "Mars: An instance-aware, modular and realistic simulator for autonomous driving," in *CAAI*, pp. 3–15, 2023.
- [107] Z. Yang, Y. Chen, J. Wang, S. Manivasagam, W.-C. Ma, A. J. Yang, and R. Urtasun, "Unisim: A neural closed-loop sensor simulator," in *CVPR*, pp. 1389–1399, 2023.
- [108] Z. Xie, J. Zhang, W. Li, F. Zhang, and L. Zhang, "S-nerf: Neural radiance fields for street views," in *ICLR*, 2023.
- [109] T. Deng, S. Liu, X. Wang, Y. Liu, D. Wang, and W. Chen, "Prosgnerf: Progressive dynamic neural scene graph with frequency modulated auto-encoder in urban scenes," *ArXiv Prepr. ArXiv231209076*, 2023.
- [110] T. Fischer, L. Porzi, S. R. Buló, M. Pollefeys, and P. Kotschieder, "Multi-level neural scene graphs for dynamic urban environments," in *CVPR*, pp. 21125–21135, 2024.
- [111] A. Tonderski, C. Lindström, G. Hess, W. Ljungbergh, L. Svensson, and C. Petersson, "Neurad: Neural rendering for autonomous driving," in *CVPR*, pp. 14895–14904, 2024.
- [112] M. Khan, H. Fazlali, D. Sharma, T. Cao, D. Bai, Y. Ren, and B. Liu, "Autosplat: Constrained gaussian splatting for autonomous driving scene reconstruction," *CoRR*, 2024.
- [113] S.-Y. Su, F. Yu, M. Zollhofer, and H. Rhodin, "A-nerf: Articulated neural radiance fields for learning human shape, appearance, and pose," *NeurIPS*, vol. 34, pp. 12278–12291, 2021.
- [114] A. Noguchi, X. Sun, S. Lin, and T. Harada, "Neural articulated radiance field," in *ICCV*, pp. 5762–5772, 2021.
- [115] S. Peng, J. Dong, Q. Wang, S. Zhang, Q. Shuai, X. Zhou, and H. Bao, "Animatable neural radiance fields for modeling dynamic human bodies," in *ICCV*, pp. 14314–14323, 2021.
- [116] Y. Kwon, D. Kim, D. Ceylan, and H. Fuchs, "Neural human performer: Learning generalizable radiance fields for human performance rendering," *NeurIPS*, vol. 34, pp. 24741–24752, 2021.
- [117] C. Guo, T. Jiang, X. Chen, J. Song, and O. Hilliges, "Vid2avatar: 3d avatar reconstruction from videos in the wild via self-supervised scene decomposition," in *CVPR*, pp. 12858–12868, 2023.
- [118] G. Moon, T. Shiratori, and S. Saito, "Expressive whole-body 3D gaussian avatar," in *ECCV*, pp. 19–35, 2024.
- [119] S. Hu, T. Hu, and Z. Liu, "Gauhuman: Articulated gaussian splatting from monocular human videos," in *CVPR*, pp. 20418–20431, 2024.
- [120] Z. Li, Z. Zheng, L. Wang, and Y. Liu, "Animatable gaussians: Learning pose-dependent gaussian maps for high-fidelity human avatar modeling," in *CVPR*, pp. 19711–19722, 2024.
- [121] L. Hu, H. Zhang, Y. Zhang, B. Zhou, B. Liu, S. Zhang, and L. Nie, "Gaussianavatar: Towards realistic human avatar modeling from a single video via animatable 3d

- gaussians," in *CVPR*, pp. 634–644, 2024.
- [122] H. Pang, H. Zhu, A. Kortylewski, C. Theobalt, and M. Habermann, "Ash: Animatable gaussian splats for efficient and photoreal human rendering," in *CVPR*, pp. 1165–1175, 2024.
- [123] C. Song, J. Wei, T. Chen, Y. Chen, C.-S. Foo, F. Liu, and G. Lin, "Moda: Modeling deformable 3d objects from casual videos," *IJCV*, pp. 1–20, 2024.
- [124] E. Corona, T. Hodan, M. Vo, F. Moreno-Noguer, C. Sweeney, R. Newcombe, and L. Ma, "Lisa: Learning implicit shape and appearance of hands," in *CVPR*, pp. 20533–20543, 2022.
- [125] X. Chen, B. Wang, and H.-Y. Shum, "Hand avatar: Free-pose hand animation and rendering from monocular video," in *CVPR*, pp. 8683–8693, 2023.
- [126] A. Mundra, J. Wang, M. Habermann, C. Theobalt, M. Elgharib, *et al.*, "Livehand: Real-time and photorealistic neural hand rendering," in *ICCV*, pp. 18035–18045, 2023.
- [127] L. Zhao, X. Lu, R. Fan, S. K. Im, and L. Wang, "Gaussian-Hand: Real-time 3D gaussian rendering for hand avatar animation," *TVCG*, 2024.
- [128] C. Pokhariya, I. N. Shah, A. Xing, Z. Li, K. Chen, A. Sharma, and S. Sridhar, "Manus: Markerless grasp capture using articulated 3d gaussians," in *CVPR*, pp. 2197–2208, 2024.
- [129] H. Luo, T. Xu, Y. Jiang, C. Zhou, Q. Qiu, Y. Zhang, W. Yang, L. Xu, and J. Yu, "Artemis: articulated neural pets with appearance and motion synthesis," *ACM TOG*, vol. 41, no. 4, pp. 1–19, 2022.
- [130] S. Wu, R. Li, T. Jakab, C. Rupprecht, and A. Vedaldi, "Magicpony: Learning articulated 3d animals in the wild," in *CVPR*, pp. 8792–8802, 2023.
- [131] S. Sinha, R. Shapovalov, J. Reizenstein, I. Rocco, N. Neverova, A. Vedaldi, and D. Novotny, "Common pets in 3d: Dynamic new-view synthesis of real-life deformable categories," in *CVPR*, pp. 4881–4891, 2023.
- [132] R. Sabathier, N. J. Mitra, and D. Novotny, "Animal avatars: Reconstructing animatable 3D animals from casual videos," in *ECCV*, pp. 270–287, 2024.
- [133] W.-C. Tseng, H.-J. Liao, L. Yen-Chen, and M. Sun, "Clanerf: Category-level articulated neural radiance field," in *ICRA*, pp. 8454–8460, 2022.
- [134] J. Liu, A. Mahdavi-Amiri, and M. Savva, "Paris: Part-level reconstruction and motion analysis for articulated objects," in *ICCV*, pp. 352–363, 2023.
- [135] A. Swaminathan, A. Gupta, K. Gupta, S. R. Maiya, V. Agarwal, and A. Shrivastava, "Leia: Latent view-invariant embeddings for implicit 3d articulation," in *ECCV*, pp. 210–227, 2024.
- [136] C. Song, J. Wei, C. S. Foo, G. Lin, and F. Liu, "Reacto: Reconstructing articulated objects from a single video," in *CVPR*, pp. 5384–5395, 2024.
- [137] Y. Liu, B. Jia, R. Lu, J. Ni, S.-C. Zhu, and S. Huang, "Artgs: Building interactable replicas of complex articulated objects via gaussian splatting," *arXiv preprint arXiv:2502.19459*, 2025.
- [138] Y. Liu, C. Qiu, and Z. Zhang, "Deep learning for 3D human pose estimation and mesh recovery: A survey," *Neurocomputing*, p. 128049, 2024.
- [139] J. J. Park, P. Florence, J. Straub, R. Newcombe, and S. Lovegrove, "DeepSDF: Learning continuous signed distance functions for shape representation," in *CVPR*, pp. 165–174, 2019.
- [140] L. Mescheder, M. Oechsle, M. Niemeyer, S. Nowozin, and A. Geiger, "Occupancy networks: Learning 3d reconstruction in function space," in *CVPR*, pp. 4460–4470, 2019.
- [141] W. Jiang, K. M. Yi, G. Samei, O. Tuzel, and A. Ranjan, "Neuman: Neural human radiance field from a single video," in *ECCV*, pp. 402–418, Springer, 2022.
- [142] Z. Zheng, H. Huang, T. Yu, H. Zhang, Y. Guo, and Y. Liu, "Structured local radiance fields for human avatar modeling," in *CVPR*, pp. 15893–15903, 2022.
- [143] Y. Jiang, K. Yao, Z. Su, Z. Shen, H. Luo, and L. Xu, "Instant-NVR: Instant neural volumetric rendering for human-object interactions from monocular RGBD stream," in *CVPR*, pp. 595–605, 2023.
- [144] T. Jiang, X. Chen, J. Song, and O. Hilliges, "Instantavatar: Learning avatars from monocular video in 60 seconds," in *CVPR*, pp. 16922–16932, 2023.
- [145] X. Chen, Y. Zheng, M. J. Black, O. Hilliges, and A. Geiger, "Snarf: Differentiable forward skinning for animating non-rigid neural implicit shapes," in *ICCV*, pp. 11594–11604, 2021.
- [146] X. Chen, T. Jiang, J. Song, M. Rietmann, A. Geiger, M. J. Black, and O. Hilliges, "Fast-SNARF: A fast deformer for articulated neural fields," *TPAMI*, vol. 45, no. 10, pp. 11796–11809, 2023.
- [147] Z. Dong, C. Guo, J. Song, X. Chen, A. Geiger, and O. Hilliges, "Pina: Learning a personalized implicit neural avatar from a single rgb-d video sequence," in *CVPR*, pp. 20470–20480, 2022.
- [148] K. Shen, C. Guo, M. Kaufmann, J. J. Zarate, J. Valentin, J. Song, and O. Hilliges, "X-avatar: Expressive human avatars," in *CVPR*, pp. 16911–16921, 2023.
- [149] W. Cheng, S. Xu, J. Piao, C. Qian, W. Wu, K.-Y. Lin, and H. Li, "Generalizable neural performer: Learning robust radiance fields for human novel view synthesis," *ArXiv Prepr. ArXiv220411798*, 2022.
- [150] A. Raj, M. Zollhofer, T. Simon, J. Saragih, S. Saito, J. Hays, and S. Lombardi, "Pixel-aligned volumetric avatars," in *CVPR*, pp. 11733–11742, 2021.
- [151] A. Yu, V. Ye, M. Tancik, and A. Kanazawa, "pixelnerf: Neural radiance fields from one or few images," in *CVPR*, pp. 4578–4587, 2021.
- [152] Z. Xu, S. Peng, H. Lin, G. He, J. Sun, Y. Shen, H. Bao, and X. Zhou, "4k4d: Real-time 4d view synthesis at 4k resolution," in *CVPR*, pp. 20029–20040, 2024.
- [153] M. Habermann, L. Liu, W. Xu, M. Zollhofer, G. Pons-Moll, and C. Theobalt, "Real-time deep dynamic characters," *ACM TOG*, vol. 40, no. 4, pp. 1–16, 2021.
- [154] Y. Xu, K. Ye, T. Shao, and Y. Weng, "Animatable 3D Gaussians for modeling dynamic humans," *Front. Comput. Sci.*, vol. 19, no. 9, pp. 1–11, 2025.
- [155] R. Jena, G. S. Iyer, S. Choudhary, B. Smith, P. Chaudhari, and J. Gee, "Splatarmor: Articulated gaussian splatting for animatable humans from monocular rgb videos," *ArXiv Prepr. ArXiv231110812*, 2023.
- [156] Z. Shao, Z. Wang, Z. Li, D. Wang, X. Lin, Y. Zhang, M. Fan, and Z. Wang, "Splattingavatar: Realistic real-time human avatars with mesh-embedded gaussian splatting," in *CVPR*, pp. 1606–1616, 2024.
- [157] J. Wen, X. Zhao, Z. Ren, A. G. Schwing, and S. Wang, "Gomavatar: Efficient animatable human modeling from monocular video using gaussians-on-mesh," in *CVPR*, pp. 2059–2069, 2024.
- [158] T. Zhang, Q. Gao, W. Li, L. Liu, and B. Chen, "Bags: Building animatable gaussian splatting from a monocular video with diffusion priors," *CoRR*, 2024.
- [159] C. Geng, S. Peng, Z. Xu, H. Bao, and X. Zhou, "Learning neural volumetric representations of dynamic humans in minutes," in *CVPR*, pp. 8759–8770, 2023.
- [160] B. Deng, J. P. Lewis, T. Jeruzalski, G. Pons-Moll, G. Hinton, M. Norouzi, and A. Tagliasacchi, "Nasa neural articulated shape approximation," in *ECCV*, pp. 612–628, Springer, 2020.
- [161] G. Yang, D. Sun, V. Jampani, D. Vlasic, F. Cole, H. Chang, D. Ramanan, W. T. Freeman, and C. Liu, "Lasr: Learning articulated shape reconstruction from a monocular video," in *CVPR*, pp. 15980–15989, 2021.

- [162] G. Yang, D. Sun, V. Jampani, D. Vlasic, F. Cole, C. Liu, and D. Ramanan, "Viser: Video-specific surface embeddings for articulated 3d shape reconstruction," *NeurIPS*, vol. 34, pp. 19326–19338, 2021.
- [163] N. Neverova, D. Novotny, M. Szafraniec, V. Khalidov, P. Labatut, and A. Vedaldi, "Continuous surface embeddings," *NeurIPS*, vol. 33, pp. 17258–17270, 2020.
- [164] X. Zheng, C. Wen, Z. Su, Z. Xu, Z. Li, Y. Zhao, and Z. Xue, "Ohta: One-shot hand avatar via data-driven implicit priors," in *CVPR*, pp. 799–810, 2024.
- [165] Z. Guo, W. Zhou, M. Wang, L. Li, and H. Li, "HandNeRF: Neural radiance fields for animatable interacting hands," in *CVPR*, pp. 21078–21087, 2023.
- [166] N. Qian, J. Wang, F. Mueller, F. Bernard, V. Golyanik, and C. Theobalt, "Html: A parametric hand texture model for 3d hand reconstruction and personalization," in *ECCV*, pp. 54–71, 2020.
- [167] K. Karunratanakul, S. Prokudin, O. Hilliges, and S. Tang, "Harp: Personalized hand reconstruction from a monocular rgb video," in *CVPR*, pp. 12802–12813, 2023.
- [168] Z. Chen, G. Moon, K. Guo, C. Cao, S. Pidhorskyi, T. Simon, R. Joshi, Y. Dong, Y. Xu, B. Pires, *et al.*, "URhand: Universal relightable hands," in *CVPR*, pp. 119–129, 2024.
- [169] S. Iwase, S. Saito, T. Simon, S. Lombardi, T. Bagautdinov, R. Joshi, F. Prada, T. Shiratori, Y. Sheikh, and J. Saragih, "Relightablehands: Efficient neural relighting of articulated hand models," in *CVPR*, pp. 16663–16673, 2023.
- [170] P. Kalshetti and P. Chaudhuri, "HandRT: Simultaneous hand shape and appearance reconstruction with pose tracking from monocular RGB-d video," *TPAMI*, 2025.
- [171] J. Lee, M. Sung, H. Choi, and T.-K. Kim, "Im2hands: Learning attentive implicit representation of interacting two-hand shapes," in *CVPR*, pp. 21169–21178, 2023.
- [172] Y. Ye, A. Gupta, and S. Tulsiani, "What's in your hands? 3d reconstruction of generic objects in hands," in *CVPR*, pp. 3895–3905, 2022.
- [173] Z. Tu, Z. Huang, Y. Chen, D. Kang, L. Bao, B. Yang, and J. Yuan, "Consistent 3d hand reconstruction in video via self-supervised learning," *TPAMI*, vol. 45, no. 8, pp. 9469–9485, 2023.
- [174] Y. Li, L. Zhang, Z. Qiu, Y. Jiang, N. Li, Y. Ma, Y. Zhang, L. Xu, and J. Yu, "Nimble: A non-rigid hand model with bones and muscles," *ACM TOG*, vol. 41, no. 4, pp. 1–16, 2022.
- [175] S. Zuffi, A. Kanazawa, D. W. Jacobs, and M. J. Black, "3d menagerie: Modeling the 3d shape and pose of animals," in *CVPR*, pp. 6365–6373, 2017.
- [176] B. Biggs, O. Boyne, J. Charles, A. Fitzgibbon, and R. Cipolla, "Who left the dogs out? 3d animal reconstruction with expectation maximization in the loop," in *ECCV*, pp. 195–211, 2020.
- [177] C.-H. Yao, W.-C. Hung, Y. Li, M. Rubinstein, M.-H. Yang, and V. Jampani, "Lassie: Learning articulated shapes from sparse image ensemble via 3d part discovery," *NeurIPS*, vol. 35, pp. 15296–15308, 2022.
- [178] Z. Li, D. Litvak, R. Li, Y. Zhang, T. Jakab, C. Rupprecht, S. Wu, A. Vedaldi, and J. Wu, "Learning the 3d fauna of the web," in *CVPR*, pp. 9752–9762, 2024.
- [179] F. Wei, R. Chabra, L. Ma, C. Lassner, M. Zollhöfer, S. Rusinkiewicz, C. Sweeney, R. Newcombe, and M. Slavcheva, "Self-supervised neural articulated shape and appearance models," in *CVPR*, pp. 15816–15826, 2022.
- [180] S. Peng, Y. Yan, Q. Shuai, H. Bao, and X. Zhou, "Representing volumetric videos as dynamic mlp maps," in *CVPR*, pp. 4252–4262, 2023.
- [181] Z. Li, Z. Chen, Z. Li, and Y. Xu, "Spacetime gaussian feature splatting for real-time dynamic view synthesis," in *CVPR*, pp. 8508–8520, 2024.
- [182] S. Wang, X. Yang, Q. Shen, Z. Jiang, and X. Wang, "Gflow: Recovering 4d world from monocular video," *CoRR*, 2024.
- [183] X. Guo, G. Chen, Y. Dai, X. Ye, J. Sun, X. Tan, and E. Ding, "Neural deformable voxel grid for fast optimization of dynamic view synthesis," in *ACCV*, pp. 3757–3775, 2022.
- [184] B. Attal, J.-B. Huang, C. Richardt, M. Zollhoefer, J. Kopf, M. O'Toole, and C. Kim, "Hyperreel: High-fidelity 6-dof video with ray-conditioned sampling," in *CVPR*, pp. 16610–16620, 2023.
- [185] F. Tian, S. Du, and Y. Duan, "Mononerf: Learning a generalizable dynamic radiance field from monocular videos," in *ICCV*, pp. 17903–17913, 2023.
- [186] K. Zhou, J.-X. Zhong, S. Shin, K. Lu, Y. Yang, A. Markham, and N. Trigoni, "Dynpoint: Dynamic neural point for view synthesis," *NeurIPS*, vol. 36, 2024.
- [187] D. Das, C. Wewer, R. Yunus, E. Ilg, and J. E. Lenssen, "Neural parametric gaussians for monocular non-rigid object reconstruction," in *CVPR*, pp. 10715–10725, 2024.
- [188] L. Wang, J. Zhang, X. Liu, F. Zhao, Y. Zhang, Y. Zhang, M. Wu, J. Yu, and L. Xu, "Fourier plenotrees for dynamic radiance field rendering in real-time," in *CVPR*, pp. 13524–13534, 2022.
- [189] A. Kratimenos, J. Lei, and K. Daniilidis, "Dynmf: Neural motion factorization for real-time dynamic view synthesis with 3d gaussian splatting," in *ECCV*, pp. 252–269, Springer, 2024.
- [190] E. ADELSON, "the plenoptic function and the elements of early vision", computational models of visual," *Processing, Chap. 1, Edited by M. Landy and JA Movshon*, 1991.
- [191] F. Wang, Z. Chen, G. Wang, Y. Song, and H. Liu, "Masked space-time hash encoding for efficient dynamic scene reconstruction," *NeurIPS*, vol. 36, 2024.
- [192] T. Wu, F. Zhong, A. Tagliasacchi, F. Cole, and C. Oztireli, "D<sup>2</sup>nerf: Self-supervised decoupling of dynamic and static objects from a monocular video," *NeurIPS*, vol. 35, pp. 32653–32666, 2022.
- [193] F. Wang, S. Tan, X. Li, Z. Tian, Y. Song, and H. Liu, "Mixed neural voxels for fast multi-view video synthesis," in *ICCV*, pp. 19706–19716, 2023.
- [194] W. Gan, H. Xu, Y. Huang, S. Chen, and N. Yokoya, "V4d: Voxel for 4d novel view synthesis," *TVCG*, 2023.
- [195] J. Yang, B. Ivanovic, O. Litany, X. Weng, S. W. Kim, B. Li, T. Che, D. Xu, S. Fidler, M. Pavone, *et al.*, "Emernerf: Emergent spatial-temporal scene decomposition via self-supervision," *CoRR*, 2023.
- [196] J. Li, Z. Song, and B. Yang, "NVFi: Neural velocity fields for 3D physics learning from dynamic videos," *NeurIPS*, vol. 36, 2024.
- [197] J.-W. Liu, Y.-P. Cao, T. Yang, Z. Xu, J. Keppo, Y. Shan, X. Qie, and M. Z. Shou, "Hosnerf: Dynamic human-object-scene neural radiance fields from a single video," in *ICCV*, pp. 18483–18494, 2023.
- [198] G. Wu, T. Yi, J. Fang, W. Liu, and X. Wang, "Fast High Dynamic Range Radiance Fields for Dynamic Scenes," in *3DV*, pp. 862–872, 2024.
- [199] H. Lin, S. Peng, Z. Xu, T. Xie, X. He, H. Bao, and X. Zhou, "High-fidelity and real-time novel view synthesis for dynamic scenes," in *SIGGRAPH Asia*, pp. 1–9, 2023.
- [200] X. Liu, Y.-W. Tai, C.-K. Tang, P. Miraldo, S. Lohit, and M. Chatterjee, "Gear-NeRF: Free-Viewpoint Rendering and Tracking with Motion-aware Spatio-Temporal Sampling," in *CVPR*, pp. 19667–19679, 2024.
- [201] S. Ramasinghe, V. Shevchenko, G. Avraham, and A. Van Den Hengel, "BLiRF: Bandlimited Radiance Fields for Dynamic Scene Modeling," in *AAAI*, vol. 38, pp. 4641–4649, 2024.
- [202] Q. Wang, V. Ye, H. Gao, J. Austin, Z. Li, and A. Kanazawa, "Shape of Motion: 4D Reconstruction from a Single Video," *ArXiv Prepr. ArXiv240713764*, 2024.
- [203] X. Guo, J. Sun, Y. Dai, G. Chen, X. Ye, X. Tan, E. Ding,

- Y. Zhang, and J. Wang, "Forward flow for novel view synthesis of dynamic scenes," in *ICCV*, pp. 16022–16033, 2023.
- [204] S. Wang, Y. Kwon, Y. Shen, Q. Zhang, A. State, J.-B. Huang, and H. Fuchs, "Learning dynamic view synthesis with few rgbd cameras," *ArXiv Prepr. ArXiv220410477*, 2022.
- [205] R. Ranftl, K. Lasinger, D. Hafner, K. Schindler, and V. Koltun, "Towards robust monocular depth estimation: Mixing datasets for zero-shot cross-dataset transfer," *TPAMI*, vol. 44, no. 3, pp. 1623–1637, 2020.
- [206] L. Yang, B. Kang, Z. Huang, X. Xu, J. Feng, and H. Zhao, "Depth anything: Unleashing the power of large-scale unlabeled data," in *CVPR*, pp. 10371–10381, 2024.
- [207] K. Deng, A. Liu, J.-Y. Zhu, and D. Ramanan, "Depth-supervised nerf: Fewer views and faster training for free," in *CVPR*, pp. 12882–12891, 2022.
- [208] Z. Yan, C. Li, and G. H. Lee, "Nerf-ds: Neural radiance fields for dynamic specular objects," in *CVPR*, pp. 8285–8295, 2023.
- [209] Y. Xiu, J. Yang, X. Cao, D. Tzionas, and M. J. Black, "Econ: Explicit clothed humans optimized via normal integration," in *CVPR*, pp. 512–523, 2023.
- [210] Y. Xiu, J. Yang, D. Tzionas, and M. J. Black, "Icon: Implicit clothed humans obtained from normals," in *CVPR*, pp. 13286–13296, IEEE, 2022.
- [211] L. Wang, X. Zhao, T. Yu, S. Wang, and Y. Liu, "Normalgan: Learning detailed 3d human from a single rgb-d image," in *ECCV*, pp. 430–446, 2020.
- [212] J. Guo, H. Chou, and N. Ding, "Enhancing neural radiance fields with depth and normal completion priors from sparse views," *arXiv preprint arXiv:2407.05666*, 2024.
- [213] J. Li, J. Zhang, X. Bai, J. Zheng, X. Ning, J. Zhou, and L. Gu, "Dngaussian: Optimizing sparse-view 3d gaussian radiance fields with global-local depth normalization," in *CVPR*, pp. 20775–20785, 2024.
- [214] M. Turkulainen, X. Ren, I. Melekhov, O. Seiskari, E. Rahtu, and J. Kannala, "Dn-splatter: Depth and normal priors for gaussian splatting and meshing," in *WACV*, pp. 2421–2431, IEEE, 2025.
- [215] W. Yin, C. Zhang, H. Chen, Z. Cai, G. Yu, K. Wang, X. Chen, and C. Shen, "Metric3d: Towards zero-shot metric 3d prediction from a single image," in *ICCV*, pp. 9043–9053, 2023.
- [216] D. Driess, Z. Huang, Y. Li, R. Tedrake, and M. Toussaint, "Learning multi-object dynamics with compositional neural radiance fields," in *CoRL*, pp. 1755–1768, PMLR, 2023.
- [217] W. Zielonka, T. Bagautdinov, S. Saito, M. Zollhöfer, J. Thies, and J. Romero, "Drivable 3d gaussian avatars," *ArXiv Prepr. ArXiv231108581*, 2023.
- [218] H. Zhao, C. Yang, H. Wang, X. Zhao, and W. Shen, "Sg-gs: Photo-realistic animatable human avatars with semantically-guided gaussian splatting," *arXiv preprint arXiv:2408.09665*, 2024.
- [219] Y. Liang, E. Laidlaw, A. Meyerowitz, S. Sridhar, and J. Tompkin, "Semantic attention flow fields for monocular dynamic scene decomposition," in *ICCV*, pp. 21797–21806, 2023.
- [220] E. Remelli, T. Bagautdinov, S. Saito, C. Wu, T. Simon, S.-E. Wei, K. Guo, Z. Cao, F. Prada, J. Saragih, *et al.*, "Drivable volumetric avatars using texel-aligned features," in *ACM SIGGRAPH*, pp. 1–9, 2022.
- [221] A. Kirillov, E. Mintun, N. Ravi, H. Mao, C. Rolland, L. Gustafson, T. Xiao, S. Whitehead, A. C. Berg, W.-Y. Lo, *et al.*, "Segment anything," in *ICCV*, pp. 4015–4026, 2023.
- [222] H. Xu, J. Zhang, J. Cai, H. Rezatofighi, F. Yu, D. Tao, and A. Geiger, "Unifying flow, stereo and depth estimation," *TPAMI*, vol. 45, no. 11, pp. 13941–13958, 2023.
- [223] J.-W. Liu, Y.-P. Cao, W. Mao, W. Zhang, D. J. Zhang, J. Keppo, Y. Shan, X. Qie, and M. Z. Shou, "Devrf: Fast deformable voxel radiance fields for dynamic scenes," *NeurIPS*, vol. 35, pp. 36762–36775, 2022.
- [224] N. Huang, X. Wei, W. Zheng, P. An, M. Lu, W. Zhan, M. Tomizuka, K. Keutzer, and S. Zhang, "S<sup>3</sup> gaussian: Self-supervised street gaussians for autonomous driving," *CoRR*, 2024.
- [225] S. Wang, V. Leroy, Y. Cabon, B. Chidlovskii, and J. Revaud, "Dust3r: Geometric 3d vision made easy," in *CVPR*, pp. 20697–20709, 2024.
- [226] J. Wang, M. Chen, N. Karaev, A. Vedaldi, C. Rupprecht, and D. Novotny, "Vggg: Visual geometry grounded transformer," *arXiv preprint arXiv:2503.11651*, 2025.
- [227] K. Liu, F. Zhan, M. Xu, C. Theobalt, L. Shao, and S. Lu, "Stylegaussian: Instant 3d style transfer with gaussian splatting," in *SIGGRAPH Asia 2024 Technical Communications*, pp. 1–4, 2024.
- [228] J.-W. Liu, Y.-P. Cao, J. Z. Wu, W. Mao, Y. Gu, R. Zhao, J. Keppo, Y. Shan, and M. Z. Shou, "Dynvideo-e: Harnessing dynamic nerf for large-scale motion-and view-change human-centric video editing," in *CVPR*, pp. 7664–7674, 2024.
- [229] J. C. Lee, D. Rho, X. Sun, J. H. Ko, and E. Park, "Compact 3D Gaussian Splatting for Static and Dynamic Radiance Fields," *ArXiv Prepr. ArXiv240803822*, 2024.
- [230] L. Roldão, N. Piasco, M. Bennehar, D. Tsishkou, *et al.*, "Rodus: Robust decomposition of static and dynamic elements in urban scenes," *CoRR*, 2024.
- [231] M. Tancik, V. Casser, X. Yan, S. Pradhan, B. Mildenhall, P. P. Srinivasan, J. T. Barron, and H. Kretzschmar, "Block-nerf: Scalable large scene neural view synthesis," in *CVPR*, pp. 8248–8258, 2022.
- [232] J. Lin, Z. Li, X. Tang, J. Liu, S. Liu, J. Liu, Y. Lu, X. Wu, S. Xu, Y. Yan, *et al.*, "Vastgaussian: Vast 3d gaussians for large scene reconstruction," in *CVPR*, pp. 5166–5175, 2024.
- [233] L. Xu, Y. Xiangli, S. Peng, X. Pan, N. Zhao, C. Theobalt, B. Dai, and D. Lin, "Grid-guided neural radiance fields for large urban scenes," in *CVPR*, pp. 8296–8306, 2023.
- [234] J. Lei, Y. Weng, A. W. Harley, L. J. Guibas, and K. Daniilidis, "Mosca: Dynamic gaussian fusion from casual videos via 4d motion scaffolds," *CoRR*, 2024.
- [235] Y. Lin, Z. Dai, S. Zhu, and Y. Yao, "Gaussian-flow: 4d reconstruction with dynamic 3d gaussian particle," in *CVPR*, pp. 21136–21145, 2024.
- [236] M. Wu and T. Tuytelaars, "Nervf: Neural video-based radiance fields for long-duration sequences," in *3DV*, pp. 1177–1187, 2024.
- [237] Z. Xu, Y. Xu, Z. Yu, S. Peng, J. Sun, H. Bao, and X. Zhou, "Representing long volumetric video with temporal gaussian hierarchy," *ACM TOG*, vol. 43, no. 6, pp. 1–18, 2024.
- [238] R. Rombach, A. Blattmann, D. Lorenz, P. Esser, and B. Ommer, "High-resolution image synthesis with latent diffusion models," in *CVPR*, pp. 10684–10695, 2022.
- [239] D. Podell, Z. English, K. Lacey, A. Blattmann, T. Dockhorn, J. Müller, J. Penna, and R. Rombach, "Sdxl: Improving latent diffusion models for high-resolution image synthesis," in *ICLR*.
- [240] C.-H. Lin, J. Gao, L. Tang, T. Takikawa, X. Zeng, X. Huang, K. Kreis, S. Fidler, M.-Y. Liu, and T.-Y. Lin, "Magic3d: High-resolution text-to-3d content creation," in *CVPR*, pp. 300–309, 2023.
- [241] A. Raj, S. Kaza, B. Poole, M. Niemeyer, N. Ruiz, B. Mildenhall, S. Zada, K. Aberman, M. Rubinstein, J. Barron, *et al.*, "Dreambooth3d: Subject-driven text-to-3d generation," in *ICCV*, pp. 2349–2359, 2023.
- [242] Y. Liu, K. Zhang, Y. Li, Z. Yan, C. Gao, R. Chen, Z. Yuan, Y. Huang, H. Sun, J. Gao, *et al.*, "Sora: A review on background, technology, limitations, and opportunities of

- large vision models," *CoRR*, 2024.
- [243] Y. Chang, X. Wang, J. Wang, Y. Wu, L. Yang, K. Zhu, H. Chen, X. Yi, C. Wang, Y. Wang, *et al.*, "A survey on evaluation of large language models," *ACM Trans. Intell. Syst. Technol.*, vol. 15, no. 3, pp. 1–45, 2024.
- [244] U. Singer, S. Sheynin, A. Polyak, O. Ashual, I. Makarov, F. Kokkinos, N. Goyal, A. Vedaldi, D. Parikh, J. Johnson, *et al.*, "Text-to-4d dynamic scene generation," in *ICML*, pp. 31915–31929, PMLR, 2023.
- [245] F. Hong, M. Zhang, L. Pan, Z. Cai, L. Yang, and Z. Liu, "Avatarclip: zero-shot text-driven generation and animation of 3d avatars," *TOG*, vol. 41, no. 4, pp. 1–19, 2022.
- [246] H. Ling, S. W. Kim, A. Torralba, S. Fidler, and K. Kreis, "Align your gaussians: Text-to-4d with dynamic 3d gaussians and composed diffusion models," in *CVPR*, pp. 8576–8588, 2024.
- [247] M. Qin, W. Li, J. Zhou, H. Wang, and H. Pfister, "Langsplat: 3d language gaussian splatting," in *CVPR*, pp. 20051–20060, 2024.